Title page

Title: A library of lineage-specific driver lines connects developing neuronal circuits to behavior in the *Drosophila* Ventral Nerve Cord.

Authors:

Jelly HM Soffers[1*], Erin Beck[1], Daniel Sytowski[1], Marianne Maughan[1], Devarakonda Devasi[1], Yi Zhu[2], Beth Wilson[2], Yu-Chieh David Chen[3], Ted Erclik[4,5], James W. Truman[6], James B. Skeath[2], Haluk Lacin [1*]

Affiliations:

1: Division of Molecular Biology and Biochemistry, School of Engineering and Biological Sciences, University of Missouri-Kansas City, Kansas City, Missouri, USA.

2: Department of Genetics, Washington University School of Medicine, St. Luis, 63110

3: Department of Biology, New York University, New York, NY 10003

4: Department of Biology and Cell, University of Toronto - Mississauga, Mississauga, ON L5L 1C6, Canada.

5: Department of Systems Biology, University of Toronto - Mississauga, Mississauga, ON L5L 1C6, Canada.

6: Department of Biology, University of Washington, Seattle, Washington 98195, USA

*: Corresponding authors: j.soffers@umkc.edu, hlhyr@umkc.edu

Abstract

Understanding the developmental trajectories of neuronal lineages is crucial for elucidating how they are assembled into functional neural networks. Studies investigating the nervous system development in model animals have focused only on a few regions of the Central Nervous System due to the limited availability of genetic drivers to target these regions throughout development and adult life. This hindered our understanding of how distinct neuronal lineages come together to form neuronal circuits during development. Here, we present a split-GAL4 library composed of driver lines, which we generated via editing the endogenous locus of the lineage specific transcription factors and demonstrate that we can use the elements of this library to specifically target the majority of individual neuronal lineages in the *Drosophila* ventral nerve cord (VNC) across development and adulthood. Using these genetic lines, we found striking morphological changes of neuronal processes within a lineage during metamorphosis. We also showed how

neurochemical features can be quickly assessed for a class of neurons expressing a specific gene. Lastly, we documented behaviors elicited in response to optogenetic activation of individual neuronal lineages and generated a comprehensive lineage-behavior map of the entire fly VNC. Looking forward, this lineage-specific driver library will provide genetic handles to address the questions emerging from the analysis of the recent VNC connectomics and transcriptomics datasets.

Introduction

Neuronal circuits are critical for every function of the nervous system, from perception and movement to cognition and emotion. Most neurons found in the adult central nervous systems (CNS) of animals are generated and assembled into circuits during development. Investigating the formation of these circuits provides valuable insights into the functional organization and operation of the nervous system, both in health and disease.

Drosophila has served as a unique model system for granular investigation of how neuronal circuits function due to its medium complexity yet rich repertoire of behaviors, and unprecedented tools for genetic manipulation. High-resolution electron microscopy data of the adult fly brain and ventral nerve cord (VNC) enable the visualization of individual neuronal morphologies and their synaptic connections (1-5). The integration of these morphological data with single-cell transcriptome profiles has put the adult fly CNS at the forefront for studies of circuit operations at the molecular level (6-9).

In *Drosophila* and other model animals, less attention has been given to how neuronal circuits develop compared to how they function, hindering our understanding of the developmental processes that instruct newly born neurons to assemble functional circuits. In *Drosophila*, the same set of neural stem cells, called neuroblasts (NB), sequentially form the larval and adult CNSs although the adult structure contains a greater number of neurons and exhibits increased complexity. Some of the embryonic-born neurons, which function in the larval CNS, are remodeled to integrate into adult circuits (10-12). The bulk of the adult neurons are born post-embryonically during larval and early pupal stages, and they fully differentiate and assemble into circuits during pupal life. This extended window of neurogenesis and neuronal maturation during the formation of the adult VNC facilitates experimental manipulations that are not feasible during the rapid period of neurogenesis in the embryo.

The fly VNC, like its vertebrate equivalent spinal cord, is compartmentalized functionally into lineally related groups of neurons, called neuronal lineages. In flies, Notch-mediated asymmetric cell division divides the neuronal population of each NB into two subclasses, called hemilineages: “A” hemilineages are composed of Notch ON cells and “B” hemilineages are composed of notch OFF cells (13-15). The adult fly VNC is composed of ~15,000 neurons, most of which are located in one of the three thoracic segments. Each thoracic hemisegment contains 34 major post-embryonic hemilineages, with some variations in the type of hemilineages and their morphology. Recent studies identified these hemilineages in the VNC Electron Microscopy (EM) volume dataset and showed that neurons within a given hemilineage exhibit a stereotyped pattern of connectivity (1, 2, 16, 17). This revealed that hemilineages display a propensity to form synaptic connections with neurons from other hemilineages, revealing a macro-connectivity among hemilineages. Hemilineage-based compartmentalization of the VNC has been also observed at the level of gene expression. Allen *et al.,* (6) assessed the transcriptome of the entire adult VNC via single-cell RNA sequencing (scRNAseq) and showed that hemilineage identity correlates highly with unique clusters of cells, which are partitioned solely based on gene expression via dimensionality reduction. Lastly, several studies employing lineage-restricted neuronal manipulations showed that the VNC hemilineages represent functional modules that control animal behavior (18-20). All these results point to that, similar to cardinal classes in the spinal cord (21-23), hemilineages in the VNC act as functional units, each responsible for controlling unique sets of specific behaviors. Thus, taking a hemilineage-based approach is essential to study the assembly of the neuronal circuits during development.

Addressing the question of how neurons in individual hemilineages develop into meaningful circuits requires genetic tools that allow for the manipulation of individual lineages throughout development. Existing genetic driver lines (GAL4, Split-GAL4, and LexA libraries) are limited in their use for developmental studies as they typically drive gene expression only during specific life stages, such as larval or adult phases, and lack the temporal stability required for comprehensive developmental analysis (24). Consequently, there is a critical need for developmentally stable and hemilineage specific driver lines, which will allow us to track, measure, activate, or inactivate genes and neuronal functions in individual lineages, thereby facilitating the identification of fundamental principles underlying circuit development.

Here, we introduce a split-GAL4 library that targets unique hemilineages in a developmentally stable manner. To achieve this, we first extended the work of Allan *et al*. (19) and analyzed the gene expression profile of the scRNAseq clusters, and validated if transcription factors (TFs) that mark clusters would also mark hemilineages. To achieve this, we tested TF expression patterns with reporter lines and antibody staining, and were able to assign 33 of the 34 major hemilineages to unique scRNAseq clusters using these markers. Then, we generated gene-specific split-GAL4 lines for 26 of these TFs via genome editing and recombination techniques. We tested the expression patterns of numerous binary combinations of split-GAL4 hemidrivers and report 44 combinations that target most of the VNC hemilineages specifically and in a developmentally stable manner. Finally, we demonstrate a few applications of these lines, including developmental studies, neurochemical mapping and an analysis of lineage-coupled behavior that extends the pioneering work of Harris *et al*. (19).

In conclusion, our split-GAL4 library enables targeted manipulation and behavioral analysis of individual hemilineages, providing resources to study the principles underlying circuit development.

Results

Intersecting the expression of *acj6* and *unc-4* with the split-GAL4 method faithfully marks hemilineage 23B throughout development and adult life.

Acj6 and Unc-4 TFs are expressed in numerous neuronal cell clusters in both the brain and the VNC (Figure 1A-B). Our prior work demonstrated that these proteins are co-expressed exclusively in hemilineage 23B neurons in the fly VNC and that this co-expression persists throughout development and adult life (25). To develop a genetic driver that targets only the 23B neurons in a temporally stable manner, we leveraged this unique co-expression pattern. We combined two techniques: the Trojan-exon-based driver for target gene transcription (26) and the split-GAL4 method (27). The split-GAL4 method works by reconstituting GAL4 function through the interaction of GAL4's DNA-binding domain (DBD) and an activation domain (AD) in cells where both transgenes are expressed. Here we used the *unc-4* split-GAL4 AD and DBD lines that we had previously generated (20) and created *Acj6* split-GAL4 lines by replacing the MIMIC insertion in the *acj6* coding intron with a Trojan exon encoding either p65.AD or GAL4-DBD via Recombinase-mediated cassette exchange (RMCE).

By combining *unc-4*-GAL4^{AD} and *acj6*-GAL4^{DBD} transgenes in the same animal with a nuclear UAS-GFP reporter gene, we specifically visualized 23B neurons in the adult CNS (Figure 1C). In the brain, we observed a small cluster of neurons expressing GFP in the subesophageal region, which is developmentally a part of VNC. Projections of these GFP-positive neurons suggest that they belong to the labial 23B lineage (Figure 1 - figure supplement-1D,E). Membrane GFP expression (UAS-myr-GFP) also highlighted axonal projections of a few leg, gustatory and antennal sensory neurons (Figure 1 - figure supplement-1D,E), which are missed with nuclear-based methods such as immunostaining for nuclear TF or nuclear GFP reporter genes, since sensory cell bodies are located outside of the CNS. The reverse combination (*unc-4*-GAL4^{DBD} and *acj6*-GAL4^{AD}) exhibited an almost identical expression pattern (not shown).

To verify that these gene-specific split-GAL4 drivers recapitulate and intersects the expression of *unc-4* and *acj6* genes, we performed immunostaining with antibodies against Acj6 and Unc-4 on embryos carrying the described transgenes and evaluated the overlap with the GFP signal. Robust GFP expression was observed in the late-stage embryo, marking segmentally repeated clusters of neurons in the VNC (Figure 1 - figure supplement-1A). All GFP-positive cells were also positive for Acj6 and Unc-4 immunostaining, indicating that these cells correspond to the embryonic progeny of NB7-4, embryonic 23B neurons (20). Occasionally, one-to-two cells per segment expressed both transcription factors but not GFP (not shown). These cells, located ventrally, are likely late-born immature neurons and their GFP expression likely lags endogenous gene expressions of Acj6 and Unc-4 due to the additional round of transcription and translation required for GFP expression. Outside of the CNS, GFP-positive sensory neurons were found in the embryonic head region, where taste organs are located (not shown). Overall, the embryonic expression analysis confirmed that *acj6*-GAL4^{DBD} and *unc-4*-GAL4^{AD} split-GAL4 combination accurately recapitulates Acj6 and Unc-4 protein expression. Also, post-embryonically the intersection of *acj6*-GAL4^{DBD} and *unc-4*-GAL4^{AD} marked 23B neurons. The only lineages that express Acj6 are 23B, 8B and 9B, and of these only the posterior-dorsal cells, corresponding to hemilineage 23B, co-stained for GFP and Acj6 in the larval and pupal VNC (Figure 1 - figure supplement-1C, D). Thus, this split-GAL4 combination effectively targets reporter expression specifically to the 23B neurons in the VNC throughout development and into adult life.

Identifying new marker genes for hemilineages and assigning hemilineages to clusters in the VNC.

The example described above demonstrated that combining the Trojan exon method with the split-GAL4 approach can generate temporally stable, lineage-specific driver lines for every hemilineage in the VNC, provided suitable pairs of genes are identified. Our prior work created a map of the expression of 20 TFs, each of which is expressed from early larval stages through adult life in most or all neurons of a small number of hemilineages in the adult VNC (20, 25, 28). When overlapped in a binary manner with each other, these TF can uniquely identify more than half of the 34 major adult VNC hemilineages, rendering them ideal genomic targets from which to create a library of split-GAL4 driver lines.

To identify unique binary gene combinations for the remainder of the hemilineages we further analyzed scRNAseq data of the adult VNC (19). This work defined 120 t-SNE clusters by unique combinations of significantly enriched genes, referred to as cluster markers. By comparing these cluster markers to established lineage markers, the Goodwin group assigned 18 hemilineages to one or more specific clusters, leaving 16 hemilineages unassigned. For example, they assigned grouped clusters 67, 93, 35 and 51 to lineage 23B. In agreement with our immunostaining that revealed that that cluster markers *acj6* and *unc-4* mark this hemilineage (Figure 1C), we report that also the expression patterns of *acj6* and *unc-4* expression overlap in this grouped scRNAseq cluster (Figure 1D). We hence continued with this approach and tested whether other cluster-specific marker genes were expressed in their corresponding hemilineages. For instance, Allen *et al.,* assigned clusters 0 and 100 to hemilineage 4B. Both clusters express *fkh, HLH4C*, and *oc* genes in addition to three additional genes: *hb9 (*also known as *exex), HGTX*, and *ap* that we had previously showed to be expressed in 4B neurons (29). Using GFP-tagged BAC reporter lines (*fkh*-GFP, *oc*-GFP, and *HLH4C*-GFP; (30) combined with immunostaining for Hb9 we demonstrate that cluster markers *fkh*, *hlh4C*, and *oc* are indeed expressed in 4B neurons, in both larval and adult VNCs, validating the scRNAseq results (Figure 2A, data not shown). In addition to hemilineage 4B, Hb9 marks lineage 10B and 16B neurons (31). Hemilineage 10B was assigned to cluster 39 and hemilineage 16B to cluster 5 and 46 (6). Knot (Kn) is a marker for cluster 39, and Sp1 for both clusters 5 and 46. Reporters for both genes show that Knot and Sp1 are expressed in lineage 10B and 16B neurons, respectively (Figure 2B, C). Therefore, when a cluster marker, or marker combination, is uniquely associated with a hemilineage, it accurately marks this hemilineage.

To identify the clusters that correspond to the remaining 16 hemilineages not assigned by Allen *et al.,* we focused on the orphan clusters. For example, glutamatergic clusters 15 and 86, which

are adjacent in the t-SNE plot, are the only glutamatergic populations expressing Sox21a. To identify the lineage identity of these clusters, we studied the morphology of the Sox21a-positive neurons in the VNC by expressing membrane-bound GFP under the control of a CRIMIC line reporting Sox21a expression (Figure 2D). This marked a group of ventral and anterior Sox21a-positive neuronal cell bodies situated near the midline in each hemisegment of the larval and adult VNC (Figure 2D). Their processes project dorsally and then sharply turn upon reaching the dorsal surface of the neuropil. Based on their glutamatergic neurotransmitter identity and specific morphology, which matches previously documented 2A neurons (19, 32), we assigned these clusters to hemilineage 2A.

Another example is cluster 58, which among all the VNC lineages, uniquely co-expresses *unc-4* and *islet* (also known as tup) (25). We had previously studied Unc-4-positive lineages and had identified that lineage 17A is the only Unc-4-positive lineage that expresses Islet (20). To verify whether cluster 58 is composed of lineage 17A neurons, we examined the expression pattern of another transcription factor, Hmx, which is a cluster marker for cluster 58 (6) Visualization of Hmx-positive neurons with a CRIMIC line reporting *Hmx* expression revealed that their cell bodies are located on the dorsal surface of the VNC and their processes project into the ipsilateral ventromedial neuropil, and then looping dorsally (Figure 2E). This morphology is typical of 17A neurons. Additionally, we found that cluster 77 is marked with the combination of Hmx and Tup and is directly adjacent to cluster 58 in the adult VNC t-SNE plot (6). Thus, neurons of Hmx-positive clusters 58 and 77 likely belong to lineage 17A (Figure 2E). Furthermore, we noted that some TFs are expressed in a subset of neurons within a hemilineage and appeared to correspond to one of the multiple scRNAseq clusters assigned to a hemilineage. For example, hemilineage 0A contains clusters 22, 88 and 112. Of these three, Tj expression is only significant in cluster 88. We generated wild-type MARCM clones of lineage 0A, and one can see that Tj is expressed in a subset of neurons only, presumably cluster 88 (Figure 2F). In contrast other TFs (Fkh, Inv, Mab21a, HLH3b and En) mark all clusters that belong to hemilineage 0A, as revealed by scRNAseq analysis and our immunostaining-based TF expression analysis (Asterisk in Figure 2A; data not shown). In hemilineage 21A, that is composed of only one scRNAseq cluster, Tj marks nearly all cells (Figure 2G). Taken together, these data illustrate how cluster markers identified by scRNAseq data can be used to target individual hemilineages and even distinct subclasses within hemilineages.

Ultimately, we assessed the expression of 23 novel cluster-specific marker genes, all TFs, through immunohistochemistry with antibodies against the proteins of interest and/or reporter lines that accurately recapitulate target gene expression (Table 1). This effort allowed us to assign at least one cluster to 15 of the 16 previously unassigned hemilineages in the scRNAseq data (6) (Table 1). This implies that we now have transcription profiles for 33 of the 34 major hemilineages in the VNC, which facilitates the design of lineage-specific split-GAL4 combinations. The only exception is hemilineage 18B, which remains unassigned to any scRNAseq clusters.

Building specific and temporally stable driver lines for hemilineages in the VNC.

We have generated split-GAL4 driver lines by editing the genomic locus of the TFs identified above and created a library of driver lines that can target 32 out of 34 hemilineages in the VNC (Figure 3, Figure 3 - figure supplement 1, Key Resources Table, Table 1). To edit the TF locus, wherever possible we exchanged the intronic cassette of previously engineered MIMIC or CRIMIC lines with a split-GAL4 coding Trojan exon (See Methods). For genes lacking established MIMIC or CRIMIC lines, we used CRISPR/Cas9 mediated gene editing via homology directed repair (HDR) to insert a Trojan exon carrying either DBD or AD split-GAL4 into a coding intron of the target gene and introduced attP sites to facilitate future cassette exchange with any other designer exon via phiC31 mediated cassette exchange by an injection (26, 33) or simple genetic crosses (34) (Figure 3 - figure supplement 2). In select cases we inserted a Trojan exon directly in frame before the 3' UTR of the gene (Figure 3 - figure supplement 3). In total we generated 32 split-GAL4 lines for 22 genes, 19 using the MiMIC method and 13 using CRISPR editing (Key Resources Table). The CRISPR approach failed only for *tup* and *E5*.

Comprehensive testing of split-GAL4 combinations to target each hemilineage.

We tested the expression patterns of these new split-GAL4 lines, either in combination with one another, or with previously generated split-GAL4 lines (Table 1) (20, 28, 35-37). Reconstituted GAL4 was visualized by UAS-myr GFP or tdTomato and compared to the typical lineage morphologies of cell bodies and axonal trajectories to assess whether the split-GAL4 line targeted their predicted lineage. We identified 44 combinations that target specific lineages and summarize the expression pattern of each combination in Table 1. Figure 3 and Figure 3- figure supplement 1 display the larval and adult VNC expression patterns of the driver lines generated for 32 out of 34 lineages. Robust expression was observed in 27 lineages during larval development, making these lines suitable for tracking their developmental history during metamorphosis. The expressions of the lines for the remaining lineages (1B,3B,13A,13B and 24B) start during pupal

stages. (1B: *HLH4C*-GAL4^{DBD}, *H15*-GAL4^{AD}; 3B: *H15*-GAL4^{AD}, *ChAT*-GAL4^{DBD}; 13A: *dbx*-GAL4^{DBD}, *dmrt99B*-GAL4^{AD}; 13B: *vg*-GAL4^{DBD}, *d*-GAL4^{AD} or *vg*-GAL4^{DBD}, *tey*-GAL4^{AD}; 24B: *ems*-GAL4^{DBD}, *twit*-GAL4^{AD}, data not shown).

Application of developmentally stable hemilineage specific split-GAL4 lines.

Developmental studies

Characterized as inhibitory GABAergic interneurons, 9A neurons encode directional leg movements, high frequency vibration, and joint angle, and function to control leg posture (18, 19, 32). In the adult VNC, 9A neurons show a complex axonal morphology due to the presence of several classes of neurons with distinct projections (32, 38).The *Dr*-GAL4^{AD}, *gad1*-GAL4^{DBD} combination specifically targets most, if not all, 9A neurons during development and adult life (Figure 3J). Therefore, we used this split-GAL4 combination to evaluate the morphological changes in the processes of 9A neurons during metamorphosis (Figure 4).

During white pupal stages (0h APF), post-embryonic 9A neurons exhibit their expected morphology with ipsilateral processes curving around the lateral cylinder of the leg neuropil (Figure 4A, A', arrowhead) (38). We also observed another, not previously described bundle of ipsilateral projections, more dorsal and anterior, extending from the cell bodies towards the midline in the dorsal neuropil (Figure 4", arrows). These projections turn first dorsally and then curve ventrally before crossing the midline, making a hook like projection pattern. These projections are also present in the abdominal segments and appear to have mature synapses apparent from their punctate labelling (Figure 4- figure supplement 1A), suggesting that these projections belong to embryonic born 9A neurons. To further investigate lineage 9A clones in the VNC of newly hatched larvae, consisting solely of embryonic born neurons, we generated Multi-Color Flip-out Clones with 49C03-GAL4 to target NB3-5 and generate lineage 9A clones (39, 40). Embryonic Flip-out clones mirrored the hook like projection pattern mentioned above in the second abdominal segment of first instar larvae (Figure 4- figure supplement 1B). The mature neuronal processes that were visible at 0h APF disappeared at 12h APF (Figure 4B) indicating pruning of embryonic born neurons processes during this period. At 12h APF, we observed neuronal processes that were just approaching the midline in T2, whereas they had already crossed the midline in T3, indicating that the midline crossing happens around 12 h APF. At 24h APF (Figure 4C) midline crossing fibers were visible in every thoracic segment, with growth cone-like structures innervating the leg neuropil. Some processes of the predicted embryonic born 9A

neurons project anteriorly in the longitudinal commissure after making the hook shaped projection in the neuropil. At 48h APF (Figure 4D) 9A neurons appear to have adult-like morphology, indicating that axonal and dendritic projections are largely complete. In summary, using a developmentally stable 9A hemilineage specific driver, we documented morphological changes occurring during metamorphosis, providing a foundation for future functional studies.

Neurochemical mapping

Another advantage of having split-GAL4 lines for lineage specific TFs is the ability to assess neurochemical features of specific lineages or neurons expressing a specific TF in wildtype or mutant animals. We previously showed that neurons tend to use the same neurotransmitter within a hemilineage (28). For cluster markers that are expressed in multiple lineages, one can now quickly differentiate between lineages by intersecting the expression profiles of the TF and neurotransmitter usage reporter. For example, we combined a split-GAL4 line reporting the Acj-6 expression with a gene-specific split-GAL4 line reporting the expression of either gad1, ChAT or VGlut to visualize GABAergic, cholinergic, and glutamatergic populations of Acj6-positive neurons, respectively (Figure 5). In the VNC, we did not detect any GABAergic Acj6-positive neurons, however, we detected two GABAergic Acj6-positive lineages in the brain (Figure 5A). We found a single cluster of glutamatergic Acj6-positive neurons per hemisegment in the VNC, which we previously mapped to 9B neurons (28), and now we use this combination of split-GAL4 lines as a specific driver to target hemilineage 9B (Figure 5B). Similarly, we found a single glutamatergic Acj6-positive lineage located in the dorsal part of the brain (Figure 5B). Furthermore, we detected two clusters of cholinergic Acj6-positive neurons in the VNC, which represent lineages 8B and 23B in addition to some sensory neurons (Figure 5C). In the brain, we found that Acj6-positive neurons in the optic lobes are cholinergic in addition to a few clusters of neurons in the central brain which show prominent long projections. To test whether Acj6 has any role in the neurotransmitter identity of these neurons, we repeated the same experimental procedure in an *acj6* mutant background. We found no apparent differences and concluded that Acj6 is dispensable for neurotransmitter identity (not shown). In conclusion, we showed that one can quickly assay neurotransmitter or any other identity feature (e.g., neurotransmitter receptors, axon guidance molecules) in the entire CNS by simply using the split-GAL4 system and intersecting the expression of a lineage specific gene with the expression of another gene coding for neuronal identity.

Behavioral analysis with targeted lineage manipulation

Harris *et al*.(19) developed genetic tools to mark and track hemilineages from metamorphosis through adulthood and combined this with thermogenetic activation to not only visualize many hemilineages but also assess their function in decapitated flies. However, for many hemilineages, either no driver line existed or only a small portion of a lineage was targeted. To overcome these issues, we now use the new split-GAL4 combinations to manipulate eight hemilineages for which no drivers existed (0A, 1B, 4B,8B, 9B, 14A, 16B, 17A) and target lineages studied by *Harris et al*., (19) with better coverage. Our approach is also compatible with LexA-LexAop genetic layering. This allows us to remove unwanted brain expression by applying a teashirt/FLP based genetic intersection (41). A major advantage of this is that behavior can be evaluated in both decapitated and intact flies. Finally, we evaluate lineage-coupled behavior with optogenetic activation, a method that is more robust and has a better time resolution compared to thermogenetic activation (42). Our complete lineage-behavior analysis is presented in Table 3 and we summarize four examples below.

<u>Hemilineage 8B</u>

Hemilineage 8B neurons, which are cholinergic and excitatory, show complex segment-specific intersegmental projections that innervate the tectulum and leg neuropil (32). To target 8B neurons, we used *lim3*-GAL4^{DBD}, *c15*-GAL4^{AD}, which target most of the 8B neurons as well as numerous neuronal clusters in the brain (Figure 6A). We activated only 8B neurons through exclusion of brain neurons by layering *lim3*-GAL4^{DBD}, *c15*-GAL4^{AD} with a *teashirt (tsh)* driver that restricts expression of the optogenetic construct CsChrimson-mVenus to only VNC neurons (41) (Figure 6B). We observed that optogenetic stimulation triggered jump behavior in intact and decapitated animals (Figure 6C, D). Unlike 7B neuronal activation, which makes flies raise their wings before jumping, 8B activation resulted in jumping without a wing raise which is also observed with Giant Fiber (GF) induced escape (43-47).Therefore, our results suggest that 8B neurons participate in the GF-driven take-off circuit.

To investigate the relationship between 8B and the GF neurons, we analyzed the synaptic connections of the GF (DPN01) using MANC2.1 in Neuprint (48) focusing on neurons with at least five synapses, for one half of the bilateral symmetric circuit. Hemilineage 8B neurons are indeed upstream synaptic partners of the GF, with 12 neurons accounting for 12.5% of the GF synaptic inputs (Figure 6- figure supplement 1). Surprisingly, 8B neurons were also downstream synaptic partners of the GF, with 13 neurons accounting for 12.5% of the GF's synaptic outputs (Figure 6-figure supplement 2). This contribution is significant, as it is even higher than the 8.7% of synaptic output connections that a GF dedicates to innervating the tergotrochanter motor neuron, which innervates the jump muscle. We next compared if those 8B neurons that are downstream partners

of the GF also provide input to the GF. Surprisingly, the majority of 8B neurons that talk to the GF are both downstream and upstream synaptic partners. These 9 neurons make up 21.5%. and 9.1% of total GF synaptic inputs and outputs, respectively. Taken together our behavioral data and the connectome analysis suggest that a subset of 8B neurons function in the GF circuit and elicit take-off behavior.

Hemilineage 9A

Hemilineage 9A is composed of inhibitory GABAergic neurons, which integrate sensory input from proprioceptive neurons in the leg (18, 28). To activate 9A neurons we drove CsChrimson expression with *Dr*-GAL4^{AD}; *gad1*-GAL4^{DBD}. Decapitated animals exhibited erratic walking behavior with their legs extended when the stimulus lasted over three seconds, and this erratic walking immediately stopped when the stimulus ended (Figure 6E). In agreement with previous reports (18, 19), we observed that both decapitated and intact animals extended their legs in response to activation (Video 9A)

Hemilineage 12A

Hemilineage 12A neurons are cholinergic and excitatory and display segment-specific and complex intersegmental projections. We used the *unc-4*-GAL4^{DBD}; *TfAP2*-GAL4^{AD} driver line to express CsChrimson. However, none of these animals survived to adulthood, not even in the absence of retinal, the cofactor required for CsChrimson activity. To overcome this, we generated stochastic FLP-based lineage clones that expressed CsChrimson in 12A neurons in one or a few hemisegment(s). We then optogenetic activated decapitated flies and recorded their behavior, followed by dissection and immunostaining to visualized what lineage clones were responsible for the observed phenotype. We found two cases where optogenetic activation resulted in bilateral wing opening and a leg swing, and the segment and side of the 12A lineage clone matched with the leg that moved (Figure 6F, G). We also observed the following behavioral phenotypes in response to optogenetic activation, but we did not dissect the animals to further identify the lineage clone: high frequency wing beating, backward walking immediately after the stimulus termination, and abdominal extension and bending. These results indicate that 12A neurons, as expected from their complex projections, control a magnitude of behaviors.

Hemilineage 21A

Hemilineage 21A neurons are glutamatergic, likely inhibitory interneurons, and innervate the leg neuropil in all thoracic segments. To assess the behaviors executed by 21A neurons we used two

different driver lines: *Dr*-GAL4^{AD}, *ey*-GAL4^{DBD} and *Dr*-GAL4^{AD}, *tj*-GAL4^{DBD}. Both combinations target most of the 21A neurons, the latter with higher specificity, yet both lines showed consistent results upon optogenetic activation. Stimulation of either intact or decapitated animals forced the leg segments in a specific geometry (Video 21A). In tethered intact animals, whose legs are freely moving in the air, we observed a clear flexion in the femur-tibia joint (Figure 6H-J). To test whether 21A neurons are necessary for the relative femur-tibia positioning, we eliminated 21A neurons by expressing UAS-*hid* with Dr-GAL4^{AD}, ey-GAL4^{DBD}. Flies lacking 21A neurons showed aberrant walking patterns (Video 21A). We observed that femur-tibia joints of the hind legs protruded laterally compared to the control sibling flies (Figure 6, K, L). Our results showed that 21A neurons control the relative positioning of the leg segments, especially the femur and tibia.

Discussion

The ability to trace and manipulate neuronal lineages across their developmental journey is essential for investigating how they come together to form neuronal circuits. In this study, we identified marker genes to assign nearly all hemilineages to clusters within a previously published scRNAseq dataset (6). Using this information, we generated driver lines by editing the endogenous locus of selected lineage specific markers. By employing binary combinations of these lines, we constructed a comprehensive split-GAL4 library that targets nearly all hemilineages throughout development and adult life (Table 1). Finally, we demonstrate how these lines can be used to explore neuronal morphology changes across development, as well as neurochemical properties and circuit-specific behaviors for individual neuronal lineages.

Prior to our work, only half of the clusters were annotated in adult VNC scRNAseq data (6). One reason for this is that many established lineage markers, especially TFs, are expressed at low levels and do not show up robustly in scRNAseq data (6). However, some established markers robustly co-express with scRNAseq cluster markers and we found that such cluster markers can serve as novel lineage markers, exemplified by Fkh, HLH4C and Oc, which label hemilineage 4B. Furthermore, we uncovered that cluster markers from orphan clusters, i.e. clusters lacking established lineage markers, can function as lineage markers, and this enabled us to annotate all but lineage 18B to clusters in the adult VNC scRNAseq data (Table 2) (6). In addition, we found that a few clusters we mapped are likely not pure and contain cells from two different lineages. For example, we mapped clusters 8 and 53 to lineage 8B and cluster 54 to lineage 9B; but we mapped cluster 76 to both lineages as it was enriched for genes expressed in both lineages (*acj6*, *PHDP*) or 8B only (*C15*, *mab-21*) or 9B only (Drgx, *sens-2, HLH4C, tup)*. Interestingly, in the t-

SNE plot, cluster 54 of glutamatergic 9B neurons is positioned in close proximity to the cholinergic 8B neurons and separated from other glutamatergic interneuronal clusters, which are present as a big multi-cluster. This clustering pattern reveals a substantial transcriptome similarity between 8B and 9B neurons despite their different neurotransmitter identities.

We aimed to identify specific markers that label most, if not all, neurons within a hemilineage across all lineages throughout development and adulthood (Table1). Overall, we have at least one driver line combination for each 32 hemilineages with which one can track individual lineages during development. A few of our driver line combinations mark off target neurons in addition to the target hemilineage. For example, our current driver lines for 3A and 3B hemilineages mark additional lineages. Since target and off-target lineages in these cases can be separated anatomically, these lines can still be used to follow 3A and 3B lineages during development. For functional studies, specific lineage clones can be generated with these lines as we showed for 12A hemilineage (Figure 6F, G). The only hemilineage for which we lack a driver line is 18B, though, we can follow this lineage during development using the reporter immortalization technique, which targets the progenitor NB with a specific GAL4 driver and irreversibly labels the entire progeny (28). We also encountered that certain drivers, especially those associated with neurotransmitter genes (e.g., *Dr*-GAL4^{AD}, *gad1*-GAL4^{DBD} and *H15*-GAL4^{AD}, *ChaT*-GAL4^{DBD}), targeted a small subset of neurons within a lineage during larval stages before marking nearly the entire lineage during early pupal stages. This is expected as the onset of expression of neurotransmitter genes is later than that of the identity promoting TFs and can be used to one's advantage to manipulate lineages during specific times of development. We also encountered off-target effects. The split-GAL4 driver combination of *H15*-GAL4^{AD}, *ChaT*-GAL4^{DBD} for example should target only 3A neurons, yet also exhibited off-target expression in lineages 7B and 12A. *H15* has a long 3' UTRs and is subject to post translational regulation, at least during embryogenesis (49), and we suspect that the hsp70 terminator in the Trojan exon disrupts 3' UTR-mediated mechanisms of posttranscriptional regulation. To utilize such genes as driver lines it is advisable to use strategies that preserve host gene 3' UTRs.

We leveraged this new split-GAL4 library to analyze behaviors controlled by individual hemilineages using optogenetic activation to reproduce and complement the findings of a previous study, which employed a sophisticated genetic system to the role of many, though not all, VNC hemilineages via thermogenetic activation (19). Our data is in agreement with this study for many hemilineages. However, we did observe key differences that are likely due to the

inherent differences of activation techniques. Our work characterized the behaviors elicited in response to optogenetic activation for eight hemilineages for which previously no drivers existed (0A, 1B, 4B, 8B, 9B, 14A, 16B, 17A) (Table 3). Higher specificity of our driver lines also enabled us to refine hemilineage 11A and hemilineage 11B specific behaviors, for which Harris *et al*. used drivers targeting the entire lineage, encompassing both A and B neuronal populations. Thus, our study extended the work of Harris et al., and brought the lineage-behavior map to completion, making the fly VNC the first complex nervous system to have a fully mapped, lineage-based connection to specific behaviors.

Although most of our driver lines are specific to individual hemilineages in the VNC, several of them showed extensive expression in the brain, such as lineage 8B driver *lim-3*-GAL4^{DBD}, *c15*-GAL4^{AD}. A major advantage of our genetic system is that we can restrict the expression of these drivers to the VNC through an additional layer of intersection (41). This approach allowed us to examine the effect of specifically activating 8B VNC neurons on behavior. We found that optogenetic activation of 8B neurons elicit a robust take-off behavior, closely resembling GF induced take-off (46). This observation raises the question whether 8B neurons function in the GF circuit. Our analysis using the MANC connectome data indicated that that 8B neurons do not directly talk to the TTMn motor neurons, the main output of the escape circuit (1). However, we did observe that 8B neurons are both up and downstream synaptic partners of the GF, accounting for 25% of GF synaptic input and 12.5% of GF synaptic output. Strikingly, the majority of the 8B neurons in contact with the GF appeared to be part of a loop, as they were both upstream and downstream synaptic partners of the GF. Hemilineage 8B neurons also receive leg proprioceptive input and display interconnectivity within their lineage (1). Based on these findings, we speculate that linage 8B may act as an integrator and amplifier in the GF circuit. Overall, our findings demonstrate that this split-GAL4 library provides an excellent foundation for further exploration of lineage-coupled behavior.

The applicability of these tools extends beyond the VNC. A total of 24 driver lines targeted clusters of neurons in the subesophageal zone (SEZ) (Table 1). The SEZ processes mechanosensory and gustatory sensory input and controls motor output related to feeding behavior. It is anatomically part of the VNC, and consists of three segments populated by lineages that arise from NBs that are segmentally homologous to those found in the thoracic and abdominal segments of the VNC (50-52). A key difference is that only a small number of NBs pairs survive in the SEZ (31). The SEZ NBs are expected to express a similar set of TFs as their thoracic

counterparts. Therefore, these TF and their corresponding split-GAL4 driver lines are excellent putative tools to target and manipulate homologous lineages in the SEZ.

Future goals are to develop reagents that can target distinct cell populations within hemilineages. Functional studies such as those by Agrawal *et al.,* (18) for lineage 13B, 10B and 9A demonstrated clear heterogeneity within these hemilineages. In agreement with this, we found many transcription factors are expressed in a subset of neurons within a hemilineage e.g., Tj in 0A (Figure 2F) and Tey in 4B (not shown). In fact, when assigning clusters to hemilineages, it becomes apparent that most hemilineages are composed of closely related clusters, indicating that hemilineages can be further divided into subclasses. Additional driver lines leveraging the LexA system for subclass-defining factors can be introduced as another layer of intersection on top of the split-GAL4 system to target distinct subclasses within hemilineages. For example, one can take advantage of the birth-order temporal gene, Chinmo (53), to restrict the driver activity to the early born neurons within a hemilineage. Similarly, one can target circuits in selected VNC segments by employing Hox gene drivers as additional layer of intersection, as these driver lines target the VNC segments differentially (54).

In conclusion, our study underscores the potential of temporally stable driver lines to unravel neuronal lineage complexities and offers a foundation for future research into neural circuit formation and functional maturation. Furthermore, our lineage-specific driver library will provide genetic handles to address the questions emerging from the analysis of the recent VNC connectomics and transcriptomics data.

Materials and Methods

Fly stocks and behavioral experiments

Fly stocks were reared on the standard cornmeal fly food at 25°C unless indicated otherwise. Fly lines used in this study are listed in the Key Resources Table. A current inventory of gene-specific split-GAL-4 lines is maintained by Yu-Chieh David Chen and Yen-Chung Chen from Claude Desplan's lab (https://www.splitgal4.org). Lines were contributed by the labs of Claude Desplan, Liqun Lue, Benjamin White, Norbert Perrimon and Haluk Lacin's laboratories. Behavior was tested at room temperature (22–25°C) 2–10 days post-eclosion.

Clonal Analysis

Wild type MARCM analysis was performed as described before (55). Animals were heat-shocked within 24 hours after egg hatching (25). Multi-Color FLP-Out NB3-5 (lineage 9) clones were generated with 49C03-GAL4 crossed to hsFlp2::PEST;; HA_V5_FLAG as described before (39, 40). 20X-UAS>dsFRT> CsChrimson mVenus_attp18, hs-Flp2PESt_attp3 X Tf-AP2-GAL4: lineage clones were generated via heat-shock within 24 hours window after egg hatching.

Gene editing

Introduction of Trojan split-GAL4 by Recombinase Mediated Cassette Exchange.

Gene-specific split-GAL4^{AD} and split-GAL4^{DBD} lines were made from MiMIC or CRIMIC lines via Trojan exon insertion as described before (26, 28, 33, 35). Briefly, pBS-KS-attB2-SA(0,1, or 2)-T2A-Gal4DBD-Hsp70 or pBS-KS-attB2-SA(0,1, or 2)-T2A-p65AD-Hsp70 were co-injected with phiC31 integrase into the respective MiMIC/CRIMIC parent stock (Key Resources Table). Transformants were identified via the absence of y+ or 3xP3-GFP markers. The correct orientation of the construct was validated by GFP signal upon crossing the putative hemidriver to a line carrying the counter hemidriver under control of the tubulin promoter and an UAS-GFP transgene (Key Resources Table).

Insertion of gene-specific Trojan split-GAL4 construct with CRISPR

Guide RNAs (gRNA) were selected to target all expressed isoforms in an amendable intronic region or to the 3' end of the gene if no suitable intron was present (e.g., *fer3 and ems*) (Key resources Table, Supplemental Methods Table 1). gRNAs were identified with CRISPR target' Finder for vas-Cas9 flies, BDSC#51324 with maximum stringency and minimal off-target effects (Supplemental Methods Table 1) (56). gRNA targeting *hb9, vg,* and *H15* were cloned into pCFD4 together with a guide RNA to linearize the donor vector (57, 58) the remainder of the guides were synthesized into pUC57_GW_OK2 (Genewiz/Azenta (Burlington, MA)).

CRISPR donors were generated using a modified version of the strategy developed by Kanca *et al..* (59). We used the Genewiz company to synthesize a DNA fragment into the EcoRV site of the pUC57-GW- OK2 vector. This fragment is made of the left and right homology arms (HA) which are immediately adjacent to the gRNA cut site and restriction enzyme sites (SacI-KpnI) between these arms (Supplemental Methods Figure 1A). We then directionally cloned the Sac1-attP-FRT-splitGAL4-FRT-attP-KpnI fragment (Supplemental Methods Figure 1B) in between the left and right HAs using the SacI and KpnI sites. Note that SacI and Kpn should only be chosen when the homology arms do not have these cut sites. To facilitate this last step, we generated

universal plasmids in each reading frame for each hemi driver, DBD and p65.AD in the original Trojan vector backbones, referred to as pBS-KS-attP2FRT2-SA-T2AGAL4[AD or DBD (0,1,2)]-hsp70 with Gibson assembly, combining the following fragments:

(i) pBS-KS backbone from the original Trojan vector (digested with SacI and KpnI).
(ii) the exon (consisting of splice acceptor, GAL4-DBD or p65.AD, and Hsp70 Poly A signal) was PCR-amplified from the original Trojan vectors (e.g., pBS-KS-attB2-SA(0)-T2A-p65AD-Hsp70) with the following primers:

F: 5' *ctagaaagtataggaacttc*GAATTC**agtcgatccaacatggcgacttg** 3'

R:5' *ctttctagagaataggaacttc*GATATC**aaacgagtttttaagcaaactcactcc** 3

Note EcoRI and EcoRV (capitalized) sites were included as a back-up strategy for replacing the Trojan exon between attP FRT if needed.
(iii) 5' SacI-attP-FRT sequence was PCR amplified from pM14 (59) with primers:

F: 5' <u>actcactatagggcgaattgGAGCTC</u>*acggacacaccgaag* 3'

R: 5' *caagtcgccatgttggatcgac 3'*

(iv) 3' FRT- attP-KpnI sequence PCR amplified from pM14 (59) with primers:

F: 5' **ggagtgagtttgcttaaaaactcgtt**tGATATC*gaagttcctattctctagaaag* 3'

R: 5' <u>cactaaagggaacaaaagctgggtacc</u>*gtactgacggacacaccgaag 3'*

Corresponding sequences from pBS-KS are underlined, pM14 are in italics, and Trojan AD/DBD are in bold; restriction enzyme sites are in all caps. All plasmids were validated by Sanger sequencing (Genewiz/Azenta (Burlington, MA).
Note that for *hb9, vg, sens-2, H15, scro, Ets21C* and *eve* we inserted the T2A- split-GAL4 ^{DBD} and/or T2A-split-GAL4$^{p65\text{-}AD}$ into the host gene intron as a Trojan exon with flanking FRT sites in a similar manner to CRIMIC lines generated by the Bellen Lab (detailed below). However, since this is problematic for FLP-dependent mosaic experiments we generated additional lines for *hb9, sens2, Ets21C eve* and *vg* lacking FRT sites by replacing the FRT flanked cassettes with the original White lab Trojan AD/DBD exons via attp-phic31 mediated recombination as described above.

<u>*Direct split-GAL4 insertion with CRISPR*</u>

For *fer3, ems, HLH4C,* we inserted T2A-GAL4^{DBD} directly in frame with the last coding exon instead of inserting it into an intron as a Trojan exon flanked by attP and FRT sites. The gRNA and entire donor region (a LHA-GAL4-DBD-RHA fragment, without attP and FRT sequences)

were synthesized in pUC57_gw_OK2, and injected into vas-Cas9 flies (w[1118]; PBac(y[+mDint2]=vas-Cas9)VK00027) by Rainbow transgenics (Camarillo, CA). Transformed animals were crossed to flies carrying Tubulin-GAL4-AD,UAS-TdTomato and offspring was scored for TdTomato expression to identify positive lines. The expression pattern of the reporter served as a verification for correct editing events; no further verification was performed.

Immunochemistry and Data Acquisition

Samples were dissected in phosphate buffered saline (PBS) and fixed with 2% paraformaldehyde in PBS for an hour at room temperature and then washed several times in PBS-TX (PBS with 1% Triton-X100) for a total 20 min. Tissues were incubated with primary antibodies (Key Resources Table) for two to four hours at room temperature or overnight 4°C. After three to four rinses with PBS-TX to remove the primary antisera, tissues were washed with PBS-TX for an hour. After wash, tissues secondary antibodies were applied for two hours at room temperature or overnight at 4°C. Tissues were washed again with PBS-TX for an hour and mounted in Vectashield or in DPX after dehydration through an ethanol series and clearing in xylene (38). Images were collected with 20X or 40X objectives using confocal microscopy. Images were processed with Image J/FIJI.

Behavioral Analysis

For optogenetic experiments, we used standard food containing 0.2 mM all-trans retinal. As a light source for optogenetic activation, we used either white light coming from the gooseneck guide attached to the halogen light box or red light obtained (Amazon-Chanzon, 50W, Led chip,620nm - 625nm / 3500 - 4000LM). Animal behaviors were recorded via a USB based Basler Camera (acA640-750um) under continuous infrared light source (Amazon- DI20 IR Illuminator).

<u>Acknowledgements</u>

We thank the Lacin laboratory members for critical reading of the manuscript, discussion and suggestions. We thank Aaron Allen and Stephen Goodwin for sharing their code for scRNAseq data analysis and sharing their fly lines prior to publication and Dorothea Godt, Angelike Stathopoulos and Gerald Campbell for gifting antibodies. Many stocks obtained from the Bloomington Drosophila Stock Center (NIH P40OD018537) were used in this study as well as

antibodies from the Developmental Studies Hybridoma Bank, created by the NICHD of the NIH and maintained at the University of Iowa, Department of Biology, Iowa City, IA 52242.

Funding:

This work was supported by grants from the National Institutes of Health to Y.C.D.C (F32EY032750 and K99EY035757), J.B.S. (R01NS036570), and to H.L. (R01NS122903).

References:

1. Marin EC, Morris BJ, Stürner T, Champion AS, Krzeminski D, Badalamente G, et al. Systematic annotation of a complete adult maleDrosophilanerve cord connectome reveals principles of functional organisation. Elife.
2. Azevedo A, Lesser E, Phelps JS, Mark B, Elabbady L, Kuroda S, et al. Connectomic reconstruction of a female Drosophila ventral nerve cord. Nature. 2024;631(8020):360-8.
3. Li F, Lindsey JW, Marin EC, Otto N, Dreher M, Dempsey G, et al. The connectome of the adult Drosophila mushroom body provides insights into function. Elife. 2020;9.
4. Scheffer LK, Xu CS, Januszewski M, Lu Z, Takemura SY, Hayworth KJ, et al. A connectome and analysis of the adult Drosophila central brain. Elife. 2020;9.
5. Schlegel P, Yin Y, Bates AS, Dorkenwald S, Eichler K, Brooks P, et al. Whole-brain annotation and multi-connectome cell typing quantifies circuit stereotypy in Drosophila. bioRxiv. 2023.
6. Allen AM, Neville MC, Birtles S, Croset V, Treiber CD, Waddell S, et al. A single-cell transcriptomic atlas of the adult Drosophila ventral nerve cord. Elife. 2020;9.
7. Bates AS, Janssens J, Jefferis GS, Aerts S. Neuronal cell types in the fly: single-cell anatomy meets single-cell genomics. Curr Opin Neurobiol. 2019;56:125-34.
8. Özel MN, Simon F, Jafari S, Holguera I, Chen YC, Benhra N, et al. Neuronal diversity and convergence in a visual system developmental atlas. Nature. 2021;589(7840):88-95.
9. Yoo J, Dombrovski M, Mirshahidi P, Nern A, LoCascio SA, Zipursky SL, et al. Brain wiring determinants uncovered by integrating connectomes and transcriptomes. Curr Biol. 2023;33(18):3998-4005.e6.
10. Prokop A, Technau GM. The origin of postembryonic neuroblasts in the ventral nerve cord of Drosophila melanogaster. Development. 1991;111(1):79-88.
11. Truman JW. Metamorphosis of the central nervous system of Drosophila. J Neurobiol. 1990;21(7):1072-84.
12. Truman JW, Bate M. Spatial and temporal patterns of neurogenesis in the central nervous system of Drosophila melanogaster. Dev Biol. 1988;125(1):145-57.
13. Skeath JB, Doe CQ. Sanpodo and Notch act in opposition to Numb to distinguish sibling neuron fates in the Drosophila CNS. Development. 1998;125(10):1857-65.
14. Spana EP, Doe CQ. Numb antagonizes Notch signaling to specify sibling neuron cell fates. Neuron. 1996;17(1):21-6.

15. Truman JW, Moats W, Altman J, Marin EC, Williams DW. Role of Notch signaling in establishing the hemilineages of secondary neurons in Drosophila melanogaster. Development. 2010;137(1):53-61.

16. Ehrhardt E, Whitehead SC, Namiki S, Minegishi R, Siwanowicz I, Feng K, et al. Single-cell type analysis of wing premotor circuits in the ventral nerve cord of Drosophila melanogaster. bioRxiv. 2023.

17. Lesser E, Azevedo AW, Phelps JS, Elabbady L, Cook A, Syed DS, et al. Synaptic architecture of leg and wing premotor control networks in Drosophila. Nature. 2024;631(8020):369-77.

18. Agrawal S, Dickinson ES, Sustar A, Gurung P, Shepherd D, Truman JW, et al. Central processing of leg proprioception in Drosophila. Elife. 2020;9.

19. Harris RM, Pfeiffer BD, Rubin GM, Truman JW. Neuron hemilineages provide the functional ground plan for the Drosophila ventral nervous system. Elife. 2015;4.

20. Lacin H, Williamson WR, Card GM, Skeath JB, Truman JW. Unc-4 acts to promote neuronal identity and development of the take-off circuit in the Drosophila CNS. Elife. 2020;9.

21. Briscoe J, Pierani A, Jessell TM, Ericson J. A homeodomain protein code specifies progenitor cell identity and neuronal fate in the ventral neural tube. Cell. 2000;101(4):435-45.

22. Jessell TM. Neuronal specification in the spinal cord: inductive signals and transcriptional codes. Nat Rev Genet. 2000;1(1):20-9.

23. Lu DC, Niu T, Alaynick WA. Molecular and cellular development of spinal cord locomotor circuitry. Front Mol Neurosci. 2015;8:25.

24. Meissner GW, Vannan A, Jeter J, Close K, DePasquale GM, Dorman Z, et al. A split-GAL4 driver line resource for Drosophila CNS cell types. eLife Sciences Publications, Ltd; 2024.

25. Lacin H, Zhu Y, Wilson BA, Skeath JB. Transcription factor expression uniquely identifies most postembryonic neuronal lineages in the Drosophila thoracic central nervous system. Development. 2014;141(5):1011-21.

26. Diao F, Ironfield H, Luan H, Diao F, Shropshire WC, Ewer J, et al. Plug-and-play genetic access to drosophila cell types using exchangeable exon cassettes. Cell Rep. 2015;10(8):1410-21.

27. Luan H, Peabody NC, Vinson CR, White BH. Refined spatial manipulation of neuronal function by combinatorial restriction of transgene expression. Neuron. 2006;52(3):425-36.

28. Lacin H, Chen HM, Long X, Singer RH, Lee T, Truman JW. Neurotransmitter identity is acquired in a lineage-restricted manner in the Drosophila CNS. Elife. 2019;8.

29. Lacin H, Zhu Y, Wilson BA, Skeath JB. dbx mediates neuronal specification and differentiation through cross-repressive, lineage-specific interactions with eve and hb9. Development. 2009;136(19):3257-66.

30. Kudron MM, Victorsen A, Gevirtzman L, Hillier LW, Fisher WW, Vafeados D, et al. The ModERN Resource: Genome-Wide Binding Profiles for Hundreds of Drosophila and Caenorhabditis elegans Transcription Factors. Genetics. 2018;208(3):937-49.

31. Kuert PA, Hartenstein V, Bello BC, Lovick JK, Reichert H. Neuroblast lineage identification and lineage-specific Hox gene action during postembryonic development of the subesophageal ganglion in the Drosophila central brain. Dev Biol. 2014;390(2):102-15.

32. Shepherd D, Sahota V, Court R, Williams DW, Truman JW. Developmental organization of central neurons in the adult Drosophila ventral nervous system. J Comp Neurol. 2019;527(15):2573-98.

33. Nagarkar-Jaiswal S, Lee PT, Campbell ME, Chen K, Anguiano-Zarate S, Gutierrez MC, et al. A library of MiMICs allows tagging of genes and reversible, spatial and temporal knockdown of proteins in Drosophila. Elife. 2015;4.

34. Li SA, Li HG, Shoji N, Desplan C, Chen Y-CD. Protocol for replacing coding intronic MiMIC and CRIMIC lines with T2A-split-GAL4 lines in Drosophila using genetic crosses. STAR Protocols. 2023;4(4):102706.

35. Chen YD, Chen YC, Rajesh R, Shoji N, Jacy M, Lacin H, et al. Using single-cell RNA sequencing to generate predictive cell-type-specific split-GAL4 reagents throughout development. Proc Natl Acad Sci U S A. 2023;120(32):e2307451120.

36. Xie Q, Brbic M, Horns F, Kolluru SS, Jones RC, Li J, et al. Temporal evolution of single-cell transcriptomes of Drosophila olfactory projection neurons. Elife. 2021;10.

37. Xie Q, Wu B, Li J, Xu C, Li H, Luginbuhl DJ, et al. Transsynaptic Fish-lips signaling prevents misconnections between nonsynaptic partner olfactory neurons. Proc Natl Acad Sci U S A. 2019;116(32):16068-73.

38. Truman JW, Schuppe H, Shepherd D, Williams DW. Developmental architecture of adult-specific lineages in the ventral CNS of Drosophila. Development. 2004;131(20):5167-84.

39. Lacin H, Truman JW. Lineage mapping identifies molecular and architectural similarities between the larval and adult Drosophila central nervous system. Elife. 2016;5:e13399.

40. Nern A, Pfeiffer BD, Rubin GM. Optimized tools for multicolor stochastic labeling reveal diverse stereotyped cell arrangements in the fly visual system. Proc Natl Acad Sci U S A. 2015;112(22):E2967-76.

41. Simpson JH. Rationally subdividing the fly nervous system with versatile expression reagents. J Neurogenet. 2016;30(3-4):185-94.

42. Klapoetke NC, Murata Y, Kim SS, Pulver SR, Birdsey-Benson A, Cho YK, et al. Independent optical excitation of distinct neural populations. Nat Methods. 2014;11(3):338-46.

43. Namiki S, Dickinson MH, Wong AM, Korff W, Card GM. The functional organization of descending sensory-motor pathways in Drosophila. Elife. 2018;7.

44. Namiki S, Ros IG, Morrow C, Rowell WJ, Card GM, Korff W, et al. A population of descending neurons that regulates the flight motor of Drosophila. Curr Biol. 2022;32(5):1189-96.e6.

45. Zabala FA, Card GM, Fontaine EI, Dickinson MH, Murray RM. Flight dynamics and control of evasive maneuvers: the fruit fly's takeoff. IEEE Trans Biomed Eng. 2009;56(9):2295-8.

46. Card G, Dickinson M. Performance trade-offs in the flight initiation of Drosophila. J Exp Biol. 2008;211(Pt 3):341-53.

47. Cheong HSJ, Eichler K, Stürner T, Asinof SK, Champion AS, Marin EC, et al. Transforming descending input into behavior: The organization of premotor circuits in the Drosophila Male Adult Nerve Cord connectome. bioRxiv. 2024:2023.06.07.543976.

48. Plaza SM, Clements J, Dolafi T, Umayam L, Neubarth NN, Scheffer LK, et al. neuPrint: An open access tool for EM connectomics. Front Neuroinform. 2022;16:896292.

49. Leal SM, Qian L, Lacin H, Bodmer R, Skeath JB. Neuromancer1 and Neuromancer2 regulate cell fate specification in the developing embryonic CNS of Drosophila melanogaster. Dev Biol. 2009;325(1):138-50.

50. Doe CQ, Goodman CS. Early events in insect neurogenesis. II. The role of cell interactions and cell lineage in the determination of neuronal precursor cells. Dev Biol. 1985;111(1):206-19.

51. Hartenstein V, Omoto JJ, Ngo KT, Wong D, Kuert PA, Reichert H, et al. Structure and development of the subesophageal zone of the Drosophila brain. I. Segmental architecture, compartmentalization, and lineage anatomy. J Comp Neurol. 2018;526(1):6-32.

52. Li HH, Kroll JR, Lennox SM, Ogundeyi O, Jeter J, Depasquale G, et al. A GAL4 driver resource for developmental and behavioral studies on the larval CNS of Drosophila. Cell Rep. 2014;8(3):897-908.

53. Zhu S, Lin S, Kao CF, Awasaki T, Chiang AS, Lee T. Gradients of the Drosophila Chinmo BTB-zinc finger protein govern neuronal temporal identity. Cell. 2006;127(2):409-22.

54. Diao F, Vasudevan D, Heckscher ES, White BH. Hox gene-specific cellular targeting using split intein Trojan exons. Proc Natl Acad Sci U S A. 2024;121(17):e2317083121.

55. Lee T, Luo L. Mosaic Analysis with a Repressible Cell Marker for Studies of Gene Function in Neuronal Morphogenesis. Neuron. 1999;22(3):451-61.

56. Gratz SJ, Ukken FP, Rubinstein CD, Thiede G, Donohue LK, Cummings AM, et al. Highly specific and efficient CRISPR/Cas9-catalyzed homology-directed repair in Drosophila. Genetics. 2014;196(4):961-71.

57. Port F, Chen HM, Lee T, Bullock SL. Optimized CRISPR/Cas tools for efficient germline and somatic genome engineering in Drosophila. Proc Natl Acad Sci U S A. 2014;111(29):E2967-76.

58. Kanca O, Zirin J, Garcia-Marques J, Knight SM, Yang-Zhou D, Amador G, et al. An efficient CRISPR-based strategy to insert small and large fragments of DNA using short homology arms. eLife. 2019;8:e51539.

59. Kanca O, Zirin J, Hu Y, Tepe B, Dutta D, Lin WW, et al. An expanded toolkit for Drosophila gene tagging using synthesized homology donor constructs for CRISPR-mediated homologous recombination. Elife. 2022;11.

Legends

Key Resources Table: Reagents used in this study.

Table 1: Overview of cluster annotation, lineage specific marker genes and tested split-GAL4 driver lines.

Table 2: Overview of behavioral phenotypes upon optogenetic stimulations of specific hemilineages.

Figure 6-Supplemental Table 1: synaptic inputs of the Giant Fiber neuron.

Figure 6-Supplemental Table 2: synaptic outputs of the Giant Fiber neuron.

Supplemental Table 1: Additional information CRISPR reagents.

Figure 1: Intersecting the expression of *acj6* and *unc-4* genes with the Split-GAL4 method faithfully marks hemilineage 23B.

(A-C) Projections of confocal stacks of the adult VNC. Magenta: CadN, green: GFP **(A)** *acj6*-GAL4 driven UAS-GFP expression marks Acj6 expressing neurons**. (B)** *unc-4*-GAL4 driven UAS-GFP expression marks Unc-4 expressing neurons. **(C)** The intersection of *acj6* and *unc-4* expression (*acj6*-GAL4^{AD}, *unc-4*-GAL4^{DBD}>UAS-GFP) marks lineage 23B neurons in the SEZ and VNC**. (D)** A partial confocal projection showing the complete overlap between GFP and Acj6 immunostainings in *acj6*-GAL4^{AD}, *unc-4*-GAL4^{DBD}-marked 23B neurons in the adult VNC (T1 and T2 segments). **(E)** scRNAseq t-SNE plot shows Acj6 and Unc-4 co-expression in a group of cell clusters.

Figure 1 - figure supplement 1: *acj6*-GAL4^{AD}, *unc-4*-GAL4^{DBD}-driven myr-GFP marks 23B neurons throughout development. **(A)** Acj6 (blue) and Unc-4 (magenta) co-expression shows robust overlap in GFP-marked embryonic progeny of NB7-4, 23B neurons, in a late embryo. **(B-C)** Acj6 (blue) expression marks 23B neurons in an early stage larval VNC **(B)** and an early stage pupal VNC **(C). (D)** This driver combination marks a cluster of SEZ neurons (arrowhead) in the adult brain, presumably SEZ 23B neurons in addition to sensory neuron afferents (arrows). **(E)** Close up of SEZ to highlight the corresponding cell bodies (arrowhead).

Figure 2: Matching the scRNAseq clusters to hemilineages. (A-C) Confocal stack of larval VNC displaying the overlapping expressions between TFs identified from scRNAsec data (Fkh, Kn, and Sp; green in **A**, **B**, and **C**, respectively) and Hb9 (magenta) in three lineages: 4B, 10B, and 16B (dashed lines). Asterisk in A indicates the Fkh^{+}Hb9^{-} 0A lineage neurons. **(D)** Sox21a-GAL4 driven UAS-GFP (green) marks lineage 2A neurons **(E)** Hmx^{GFSTF} reporter (green) marks

lineage 17A neurons. **(F, G)** Wild-type MARCM clones (green) immunostained for Tj (magenta). The insets show the clone location in the VNC counterstained with CadN (blue) **(F)** Tj marks subpopulations of neurons in lineage 0A in the T2 segment. These neurons likely belong to cluster 88, the only Tj+ 0A cluster in scRNAsec data. **(G)** Tj marks nearly all neurons of lineage 21A in the T1 segment. Lineage identification of MARCM clones were performed based on neuronal projections detailed in Truman et al., 2004. scRNAseq clusters with the corresponding lineages shown under each panel. Only one thoracic segment shown. Neuroglian specific antibody BP104 labels axon bundles of all lineages (magenta in D-E).

Figure 3: The VNC expression of select driver lines from the Split-GAL4 library targeting individual hemilineages.

Projections of confocal stacks showing the expression pattern of Split-GAL4 driven membranous GFP (green) in the larval (**A-O)** and adult VNC **(A'-O')**. Only thoracic segments are shown in the larval images **(A, A')** Hemilineage 0A, marked by *inv*-GAL4-DBD, *tj*-vp16.AD. **(B, B')** Hemilineage 1A marked by *ets21c*- GAL4-DBD, *Dr*-p65.AD. **(C-C')** Hemilineage 2A marked by sox21a GAL4-DBD, *VGlut*-p65.AD. **(D, D')** Hemilineage 4B marked by *ap*-p65.AD, *fkh*-GAL4-DBD. **(E, E')** Hemilineage 5B marked by *vg*-p65.AD, *toy*-GAL4-DBD. **(F, F')** Hemilineage 6B marked by *sens2*-p65.AD, *vg*-GAL-DBD. **(G, G')** Hemilineage 7B marked by *mab21*-GAL4-DBD, *unc-4*-p65.AD. **(H)** Hemilineage 8A marked by *ems*-GAL4-DBD, *ey*-p65.AD**. (I, I')** Hemilineage 8B marked by *lim3*-GAL4-DBD, *C15*-p65.AD**. (J, J')** Hemilineage 9A marked by *Dr*-p65.AD, *gad1*-GAL4-DBD **(K, K')** Hemilineage 9B marked by *acj6*-p65.AD, *VGlut*-GAL4-DBD. **(L, L')** Hemilineage 10B marked by *hb9*-p65.AD, *knot*-GAL4-DBD. **(M, M')** Hemilineage 12A marked by *TfAP-2*-GAL4-DBD, *unc-4*-p65.AD. **(N, N')** Hemilineage 14A marked by *Dr*-p65.AD, *toy*-GAL4-DBD. **(O, O')** Hemilineage 17A marked by *unc-4*-p.65AD, *hmx*-GAL4-DBD.

The VNC was counterstained with CadN (magenta). The target lineage is indicated on the left bottom corner of each panel. Z-projections were made of selected regions of the VNC to highlight the cell-body clustering and axonal budling.

Figure 3 - figure supplement 1: The rest of the driver lines from the Split-GAL4 library targeting individual hemilineages. Projections of confocal stacks showing the expression pattern of Split-GAL4-driven membranous GFP (green) in the larval (**A-O)** and adult VNC **(A'-O')**. Only thoracic segments shown in the larval images. **(A)** Hemilineage 1B marked by *HLH4c*-GAL4-DBD, *H15*-p65.AD. **(B)** Hemilineages 3A, 7B, and 12A are marked by *H15*-p65.AD, *ChAT*-GAL4-DBD. **(C)** Hemilineages 3B and 12B marked by *fer3*-GAL4-DBD, *cg4328*-AD**. (D)** Hemilineage 6A

marked by *mab21*-p65.AD, *toy*-GAL4-DBD. **(E)** Hemilineage 11A marked by *unc-4*-GAL4-DBD, teyVP16.AD. **(F)** Hemilineage 11B marked by *eve*-p65.AD, *gad1*-GAL4-DBD. **(G)** Hemilineage 12B marked by *HGTX*-GAL4-DBD, *gad1*-p65.AD. **(H)** Hemilineage 13A marked by *dbx*-GAL4-DBD, *dmrt*-p65.AD. **(I)** Hemilinege13B marked by *vg*-GAL4-DBD, *D*-vp16.AD. **(J)** Hemilineage 15B marked by *HGTX*-GAL4-DBD, *VGlut*-p65.AD. **(K)** Hemilineage16B marked by *hb9*-p.65AD, *VGlut*-GAL4-DBD. **(L)** Hemilineage 19A marked by *dbx*-GAL4-DBD, *scro*-p65.AD. **(M)** Hemilineage 20/22A marked by *bi*-GAL4-DBD, *shaven*-p65.AD. **(N)** Hemilineage 23B marked by *unc-4*-p65.AD, *acj6*-GAL4-DBD. **(O)** Hemilineage 24B marked by *twit*-p65.AD, *ems*-GAL4-DBD.

Figure 4: 9A neurons show profound morphological changes during development. Projection of confocal stacks showing the morphology of 9A neurons (green) marked with *Dr*-p65.AD, *gad1*-GAL4-DBD driver across different developmental time points during metamorphosis - 0 ,12, 24 and 48 hours after puparium formation (APF); the VNC is counterstained with CadN (magenta). A-D show the complete projections in T2-T3 segments. The T1 segment is also visible in **A**. (**A-D)** Transverse view of T2 segments across the entire Dorso-Ventral axis shown; Dorsal is up**. A"-D"** show a partial Z-projection of the region in T2 segments where 9A axons cross the midline. **(A, A')** At 0 h APF, postembryonic 9A neurons extend the typical ipsilateral processes curving around the lateral cylinder of the leg neuropil (arrows). Another bundle of ipsilateral projections, more dorsal and anterior, extends from the cell bodies towards the midline in the dorsal neuropil (arrowheads). **(B, B')** At 12h APF, the mature neuronal processes that were visible at 0h APF (puncta labeling of synapses, asterisks in **A'**) are no longer visible, indicating pruning of embryonic born neurons between 0-12h APF. **(B-B'')** Some neuronal processes (yellow arrowheads) cross (T3 segment) and some are in the process of crossing (T2 segment) the midline. **(C-C'').** At 24h APF, midline crossing fibers are visible in every thoracic segment (yellow arrowheads). **(D-D")** At 48h APF, 9A neurons appear to have adult-like morphology (see Fig. 3J), indicating that axonal and dendritic projections are largely complete.

Figure 4 - figure supplement 1: Hook like projections made by embryonic born lineage 9 neurons. (A) 9A neurons in an abdominal segment visualized with *Dr*-p65.AD, *gad1*-GAL4-DBD driver extend hook-like projections in a white-pupa stage animal. These processes contain mature punctae shaped synapses, indicating they belong to embryonic born neurons. **(B)** A similar projection was observed for a lineage clone generated via flip-out of lineage 9 Gal4 driver R49C03 (Lacin et al., 2016) in an abdominal segment of a newly hatched larvae. Transverse views shown.

Figure 5: Acj6^{+} neurons are either glutamatergic or cholinergic in the VNC. (A-C) Split-GAL4 line reporting Acj6 expression intersected with a cognate split-GAL4 line reporting the expression of either Gad1, ChAT or VGlut to visualize GABAergic, cholinergic, and glutamatergic populations of Acj6-positive neurons, respectively. The VNC is counterstained with CadN (magenta). **(A)** Split-GAL4 combination *acj6*-p65.AD, *gad1*-GAL4-DBD>UAS-GFP marks two GABAergic lineages in the brain. **(B)** Split-GAL4 combination *acj6*-p65.AD, *VGlut*-GAL4-DBD> UAS-GFP marks a single glutamatergic lineage in the dorsal part of the brain, and one 9A glutamatergic cluster in the VNC. **(C)** Marker combination *acj6*-p65.AD, *ChAT*-GAL4-DBD> UAS-GFP shows that the optic lobes contain cholinergic Acj6-positive neurons in addition to a few clusters of neurons with prominent long projections (arrows). Two 8B and 23B Acj6-positive clusters are cholinergic in addition to some sensory neurons (asterisks).

Figure 6: Behavioral analysis with targeted lineage manipulation. (A-D) Optogenetic activation of hemilineage 8A in the VNC triggers jump behavior. *lim3*-GAL4^{DBD}; *c15*-GAL4^{AD} driven CsChrimson::mVenus (green) targets 8B neurons in the VNC but also shows an unwanted broad brain expression **(A),** which can be suppressed via an additional layer of intersection using teashirt (tsh)-lexA driven FLP strategy (REF) **(B)**. **(C, D)** Overlay of video frames to capture the jump sequence induced by optogenetic activation of lineage 8B in the VNC. Intact flies **(C)** and decapitated flies jump without raising their wings upon optogenetic activation, but decapitated flies were slower to initiate the jump similarly. **(E)** Optogenetic activation of hemilineage 9A induces forward walking in decapitated flies. **(F, G)** Clonal stimulation of hemilineage 12A in the VNC in decapitated flies induces bilateral wing opening and single-step behavior. **(F)** Confocal stack displaying the lineage 12A clone that extends from T2 into T1 and T3. **(G)** Overlay of movie frames. The fly folds both wings outward and swings its right front leg forward upon optogenetic activation. **(H, L)** Optogenetic activation of hemilineage 21A in the VNC on a tethered, intact fly triggers flexion of the tibia-femur joint. **(H)** Without stimulus all the legs move erratically in response to being tethered. **(I)** Upon optogenetic activation all legs are pulled toward the body, the tibia-femur joints are flexed, and animals stay in this position until the end of stimulus. **(J)** Overlay of the movie shown in panel H and I, zoomed in on the left T1 leg. Note how the leg is pulled towards the body upon activation (520ms) compared to its more lateral position without activation (315 ms). **(K, L)** Elimination of 21A neurons makes hind leg femur-tibia joints protrude laterally **(L)** compared to control animals **(L).** For all overlays of movies green display frames without optogenetic activation, magenta with optogenetic activation.

Figure 6 - figure supplement 1: Giant Fiber (GF) Connectome. (A-C) Analysis of GF input connections. **(D-F)** Analysis of GF output connections. **(A)** Count of neurons per hemilineage that form synapses with GF dendrites. A total of ten hemilineages form synapses with GF dendrites. Five neurons originate from hemilineage 8B, six from hemilineage 7B, five from lineage 5B and three from lineage 21A. **(B)** Combined connectivity per hemilineage, cumulative count of synapses between GF dendrites and hemilineage neurons. The connectivity between hemilineage 8B and the GF is significant, spanning 339 synapses. Hemilineage 7B, 5B and 21A forms 45, 205 and 108 connections, respectively. **(C)** Weighted connectivity per hemilineage, calculated as the cumulative count of synapses between GF dendrites and hemilineage neurons, divided by the total number of GF output connections observed at a threshold of five synapses per neuron. Hemilineage 8B contributes heavily, making up 25% of GF input, followed by 15% from lineage 5B. Lineage 7B contributes 3.3% and lineage 21A 8%. **(D)** Count of neurons per hemilineage that form synapses with GF axons. A total of 13 hemilineages are downstream synaptic partners of the GF. Of those, the synapses formed with lineage 8B are most divergent and span 12 neurons. **(E)** Combined connectivity per hemilineage, cumulative count of synapses between GF axons and hemilineage neurons. Hemilineage 8B makes 208 synaptic contacts. Hemilineage 18B and 6B also form strong connections, 206 and 121 connections, albeit with fewer neurons (5 and 6, respectively). **(F)** Weighted connectivity per hemilineage, calculated as the cumulative count of synapses between GF axons and hemilineage neurons, divided by the total number of GF output connections observed at a threshold of five synapses per neuron. 12.5% of output GF synaptic contacts are made with hemilineage 8B, followed by 12.4 % with lineage 18B and 7.3% with lineage 6B.

Supplemental Methods Figure 1. CRISPR mediated insertion of Trojan Exons. (A) Construction of CRISPR donor plasmids. For each gene of interest (GOI) a fragment is synthesized into EcoRV restriction site of pU57_gw_OK2 as described before {Kanca, 2022 #45}. Briefly, this fragment contains a small sequence of the tRNA spacer, the gRNA against the gene of interest (GOI) (turquoise) and the Left HA and Right HA (brown) separated by a spacer containing *SacI* and *KpnI* restriction sites (black). A hemidriver cassette (gray, also see B) flanked by *SacI* and *KnpI* restriction sites is directionally cloned in between the HAs**. (B)** Six plasmids containing hemidriver cassettes (gray box) flanked by *SacI* and *KpnI* were made in the pBS-KS plasmid backbone. Each plasmid contains either a split-GAL4DBD or p65.AD in phase 0, 1 and 2. Each hemidriver furthermore contains a 5'attP and FRT sequences, followed by a linker, splice

acceptor (SA) and T2A proteolytic cleavage site. The linker length varies to keep the hemidriver in phase with the preceding exon (linker length: 24 nucleotides phase 0, 41 nucleotides phase 1 or 40 nucleotides phase2). A hsp70 termination sequence is introduced at the 3'end of the hemidriver followed by a splice donor (SD), FRT, and attP sequence Note that the DBD cassettes do not contain a splice donor to keep them consistent with previously published split-GAL4 Trojan exon donors {Diao, 2015 #39}. **(C)** The HAs promote HDR and the entire hemidriver cassette is inserted at the site of the CRISPR/CAS9 cut, targeted by recognition sequence the gRNA-GOI. The attP sites allow for future cassette exchange with RMCE and genetic crosses.

Supplemental Methods Figure 2. Direct tagging with CRISPR.

Schematic representation of the direct tagging method that establishes split-GAL4^{DBD} lines without any cloning. The gRNA against the gene of interest (GOI) cuts in the direct vicinity of the stop codon (+/- 20 nt). The left HA 3' end reaches up to, but does not include the stop codon, and the right HA 5' end starts at the first nucleotide of the 3' UTR. This ensures that the T2A-DBD fragment will be inserted at the 3' end of the gene and is translated in frame with the GOI. **(A)** Construction of the CRISPR donor for direct tagging. A fragment that contains a small portion of the tRNA spacer, the gRNA-GOI, and the LHA, T2A-DBD and RHA sequence is directly synthesized into the EcoRV site of pU57_gw_OK2. **(B)** Upon embryo injection, expression of gRNA1 linearizes the donor constructs and the LHA-T2A-DBD-RHA fragment is used for CRISPR/Cas9 guided HDR. As a result, the T2A-DBD is inserted in frame at the 3' end of the gene, and endogenous 3' UTR posttranslational regulation mechanisms remain intact.

FIGURE 1

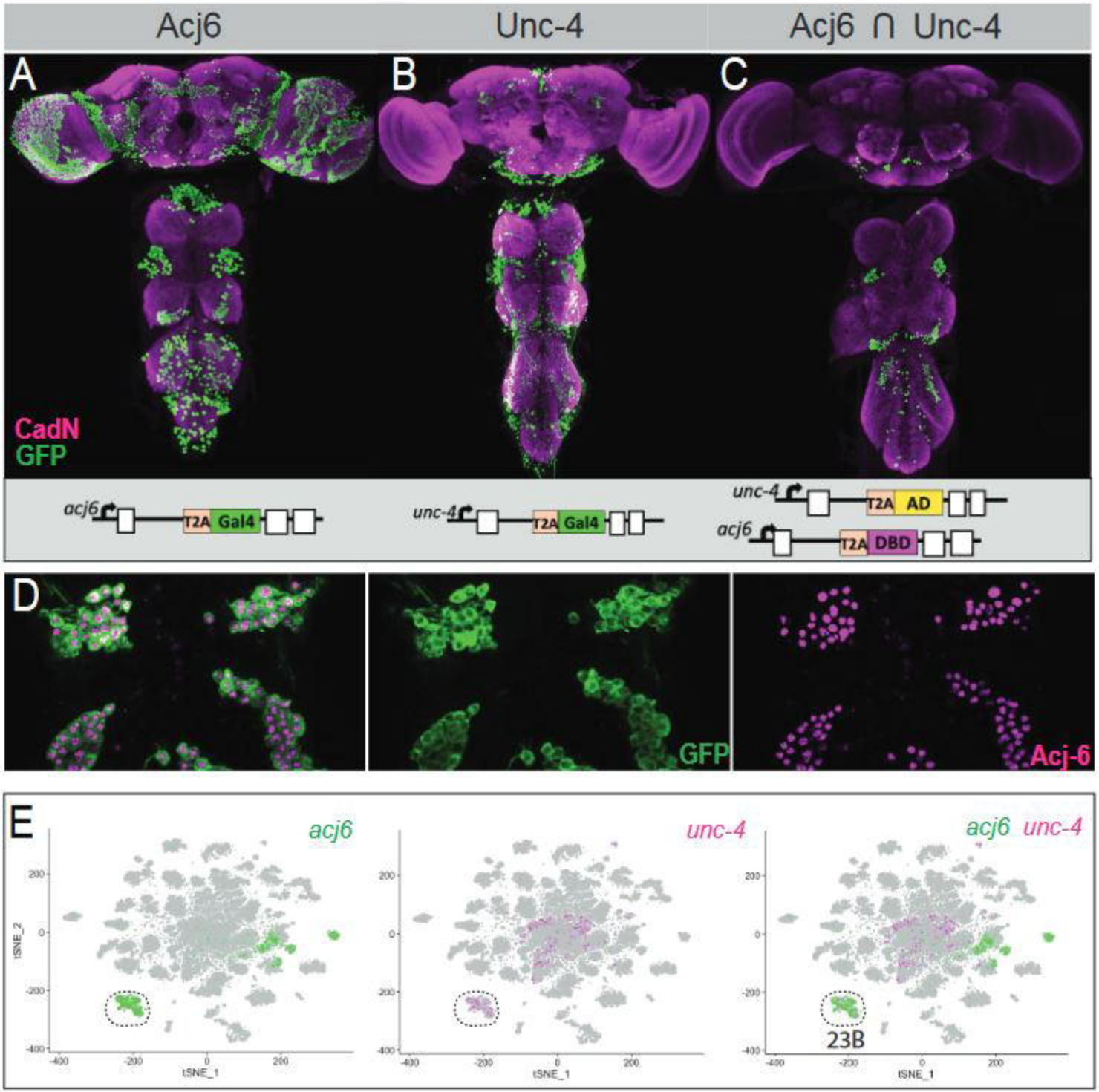
Acj6
Unc-4
Acj6 ∩ Unc-4
A
B
C
CadN
GFP
acj6
T2A
Gal4
unc-4
T2A
Gal4
unc-4
T2A
AD
acj6
T2A
DBD
D
GFP
Acj-6
E
acj6
unc-4
acj6 unc-4
23B
tSNE_1
tSNE_2

FIGURE 1-SUPP1

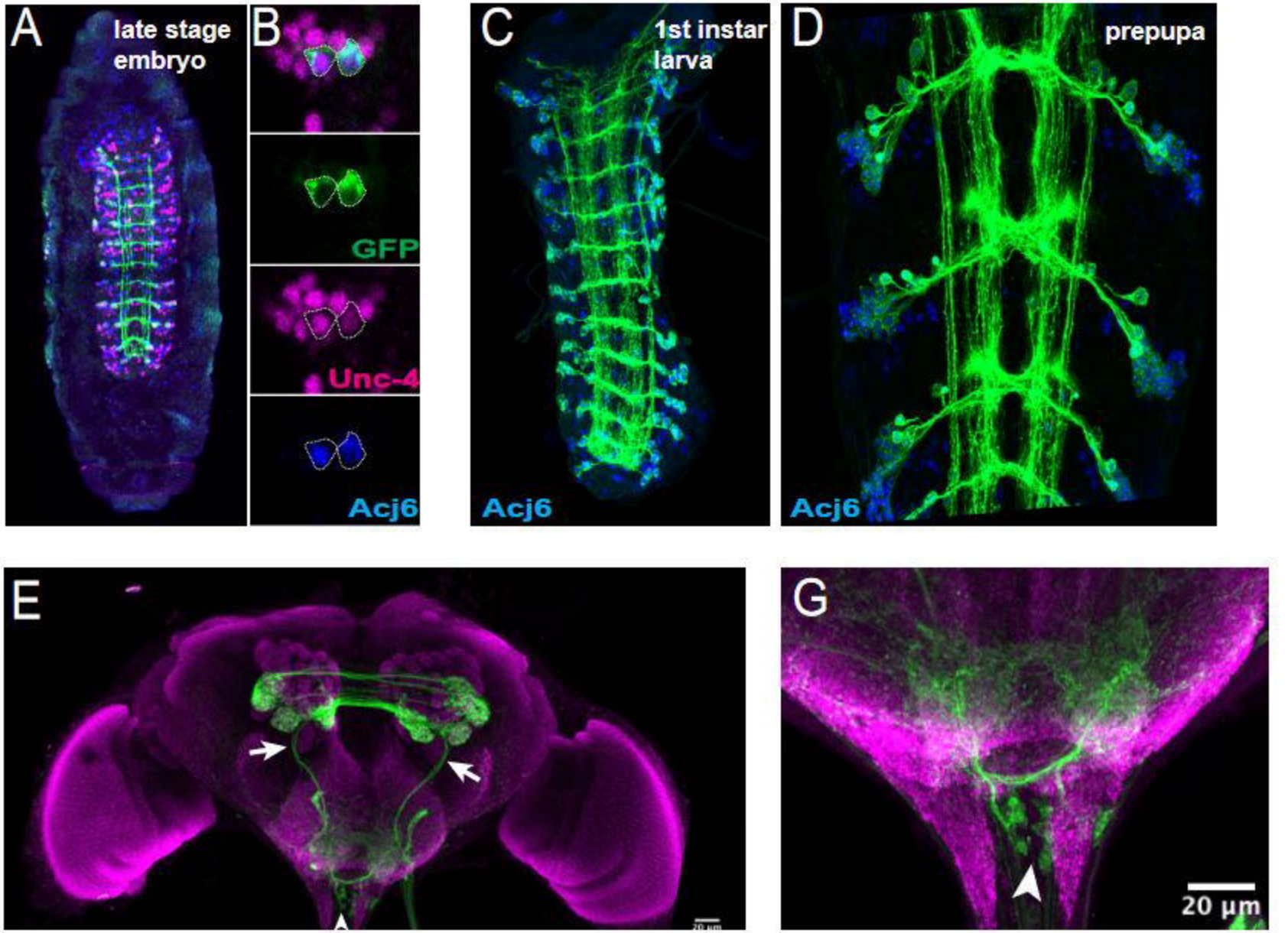

FIGURE 2

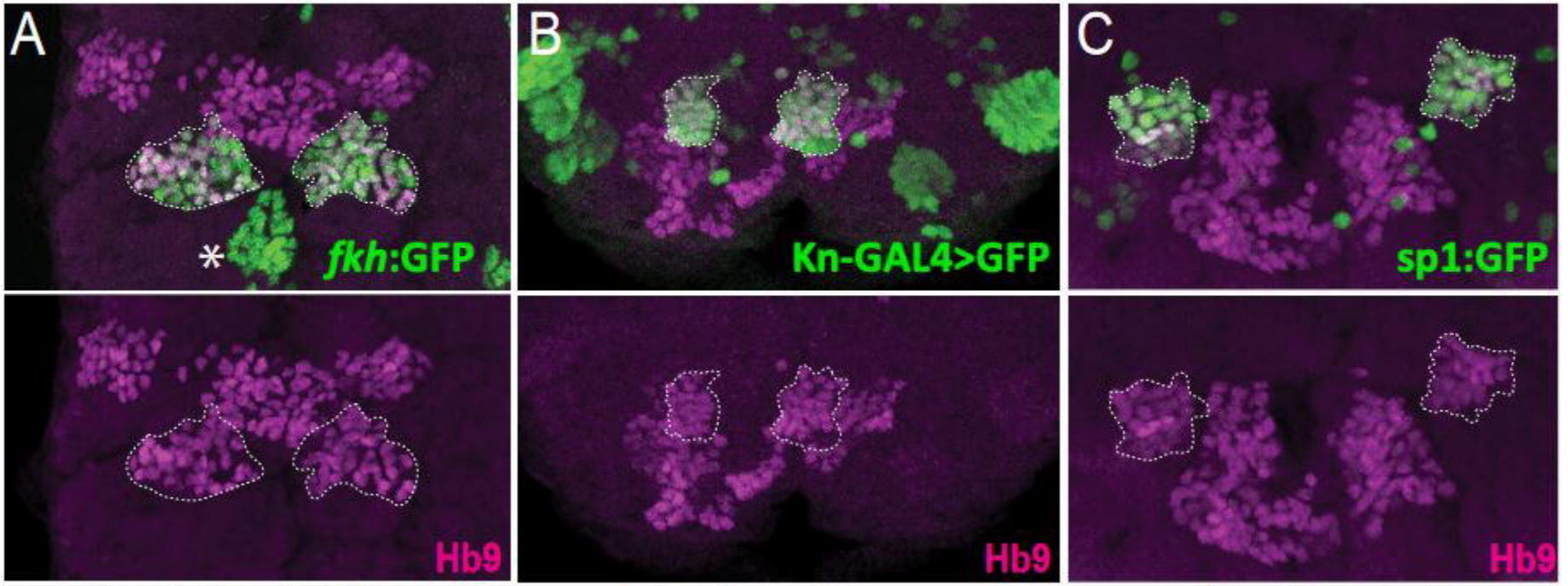

4B: clusters 0, 100 | **10B**: cluster 39 | **16B**: cluster 5, 46

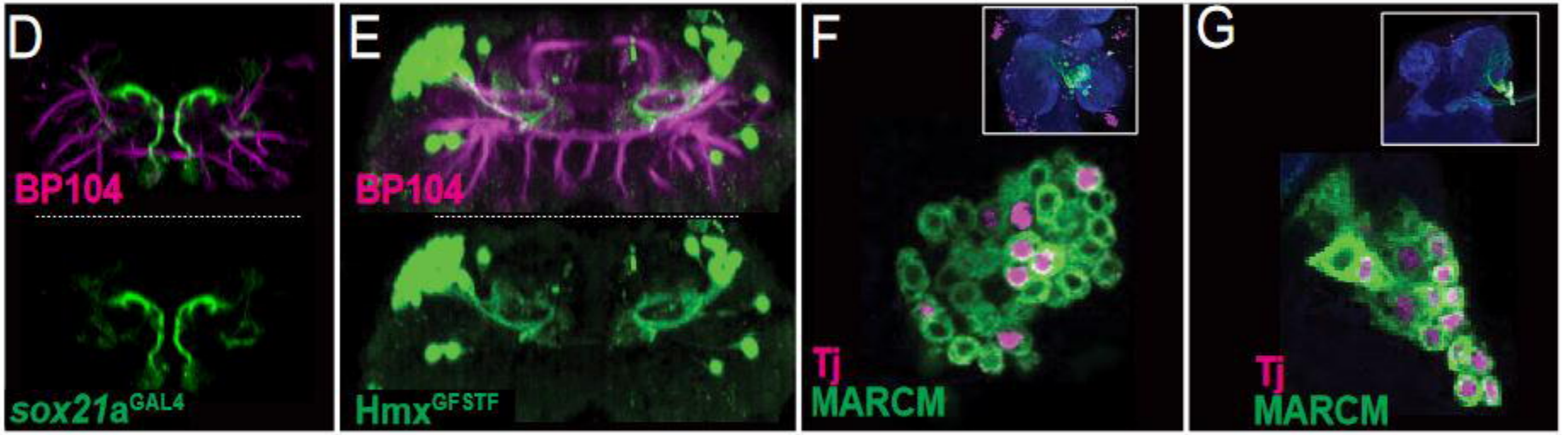

2A: clusters 15, 86 | **17A**: clusters 58 ,77 | **0A**: cluster 22,88,112 | **21A**: cluster 1

FIGURE 3

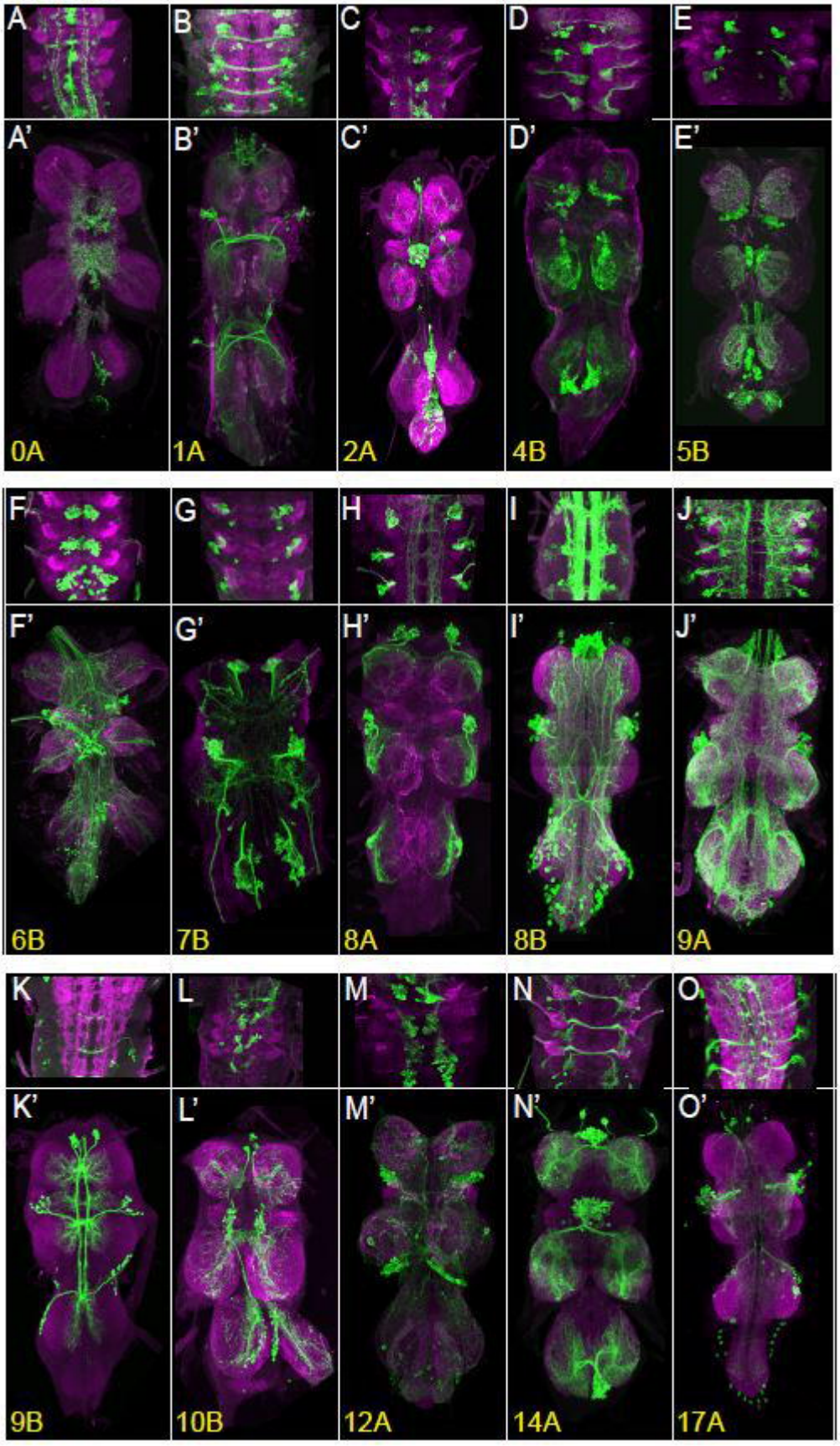
A
B
C
D
E
A'
B'
C'
D'
E'
0A
1A
2A
4B
5B
F
G
H
I
J
F'
G'
H'
I'
J'
6B
7B
8A
8B
9A
K
L
M
N
O
K'
L'
M'
N'
O'
9B
10B
12A
14A
17A

FIGURE 3-SUPP1

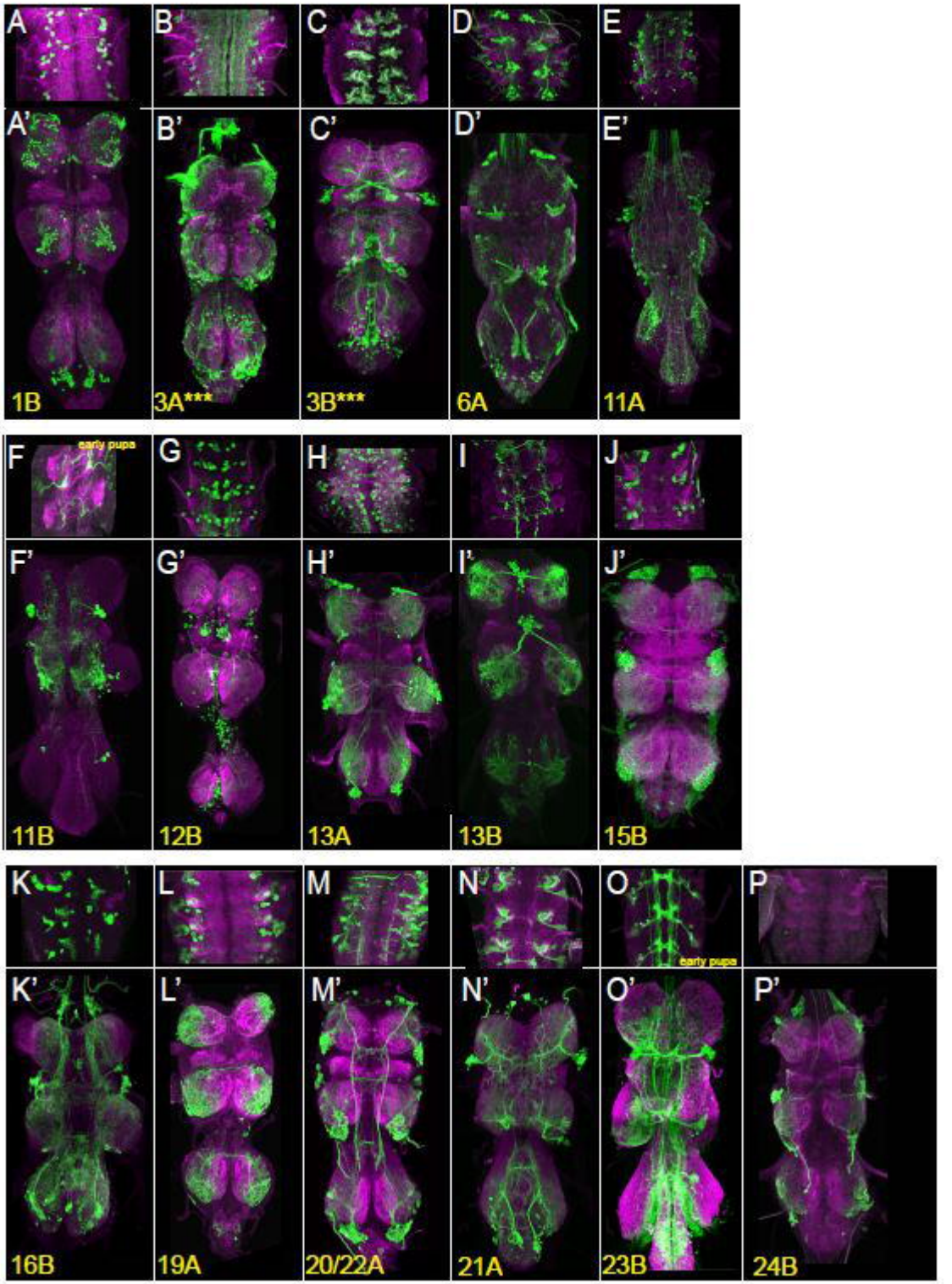

FIGURE 4

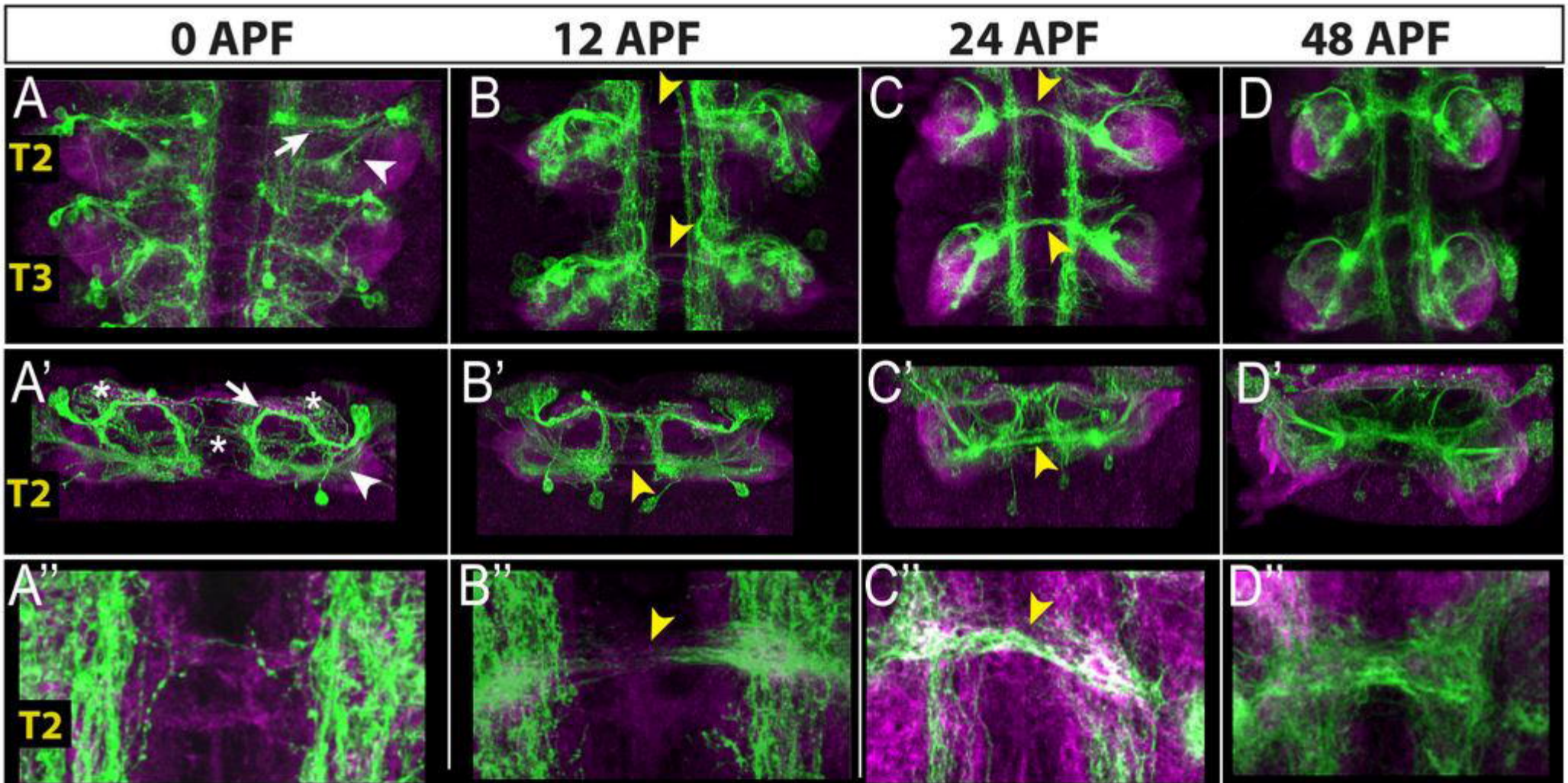

FIGURE 4-SUPP1

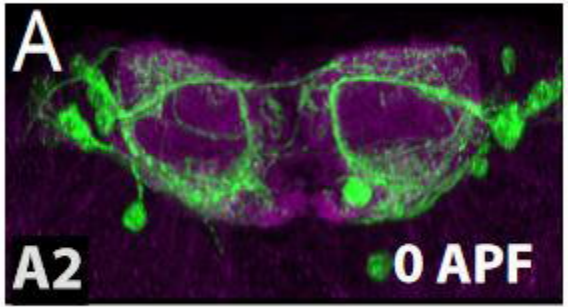

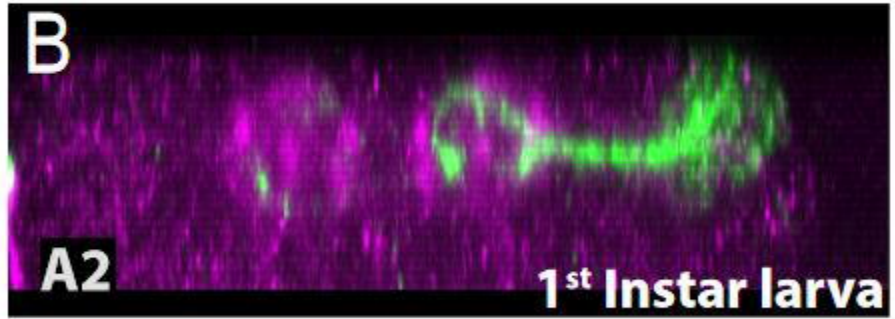

FIGURE 5

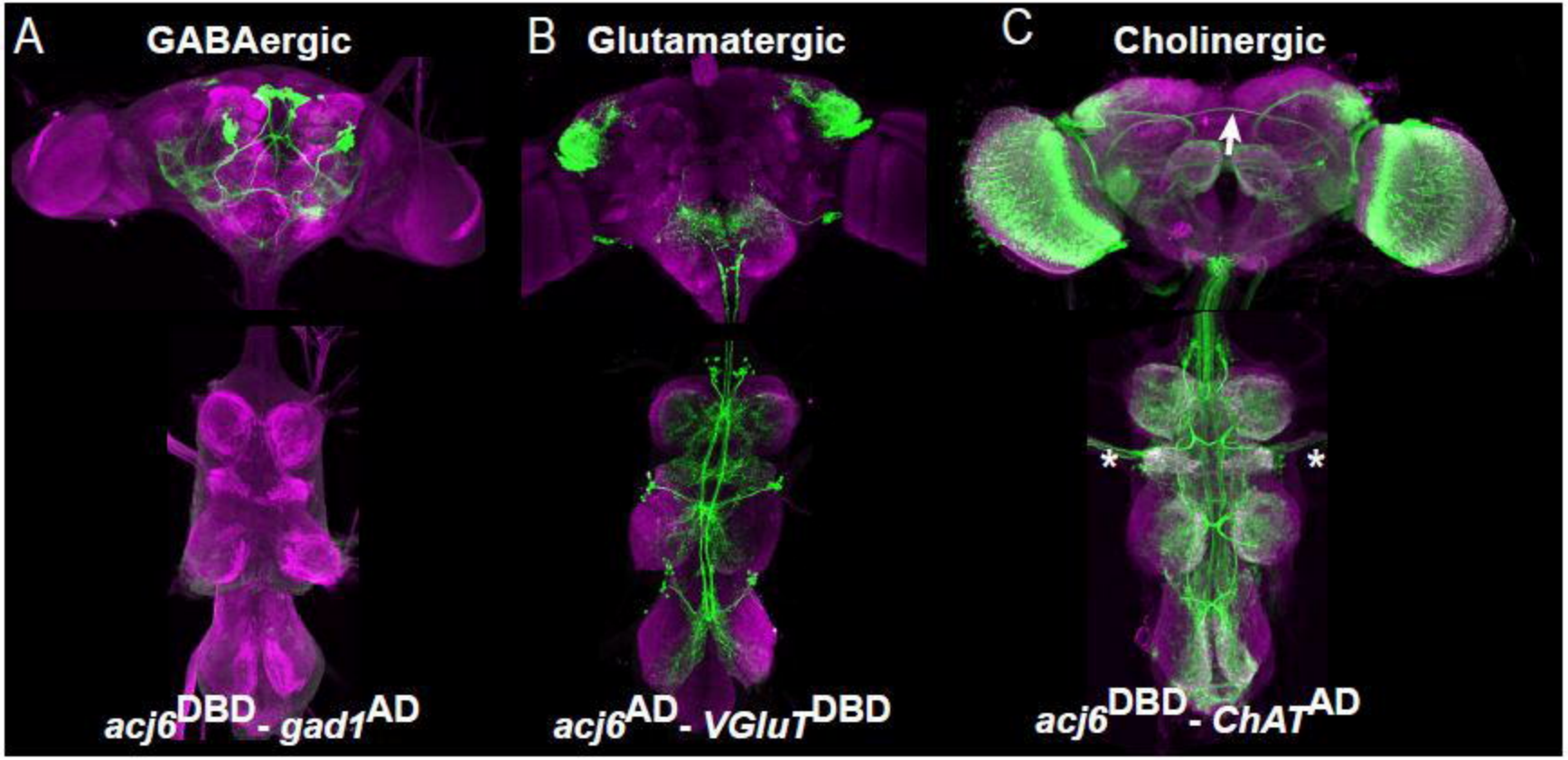
A
GABAergic
B
Glutamatergic
C
Cholinergic
*
*
acj6DBD - gad1AD
acj6AD - VGluTDBD
acj6DBD - ChATAD

FIGURE 6

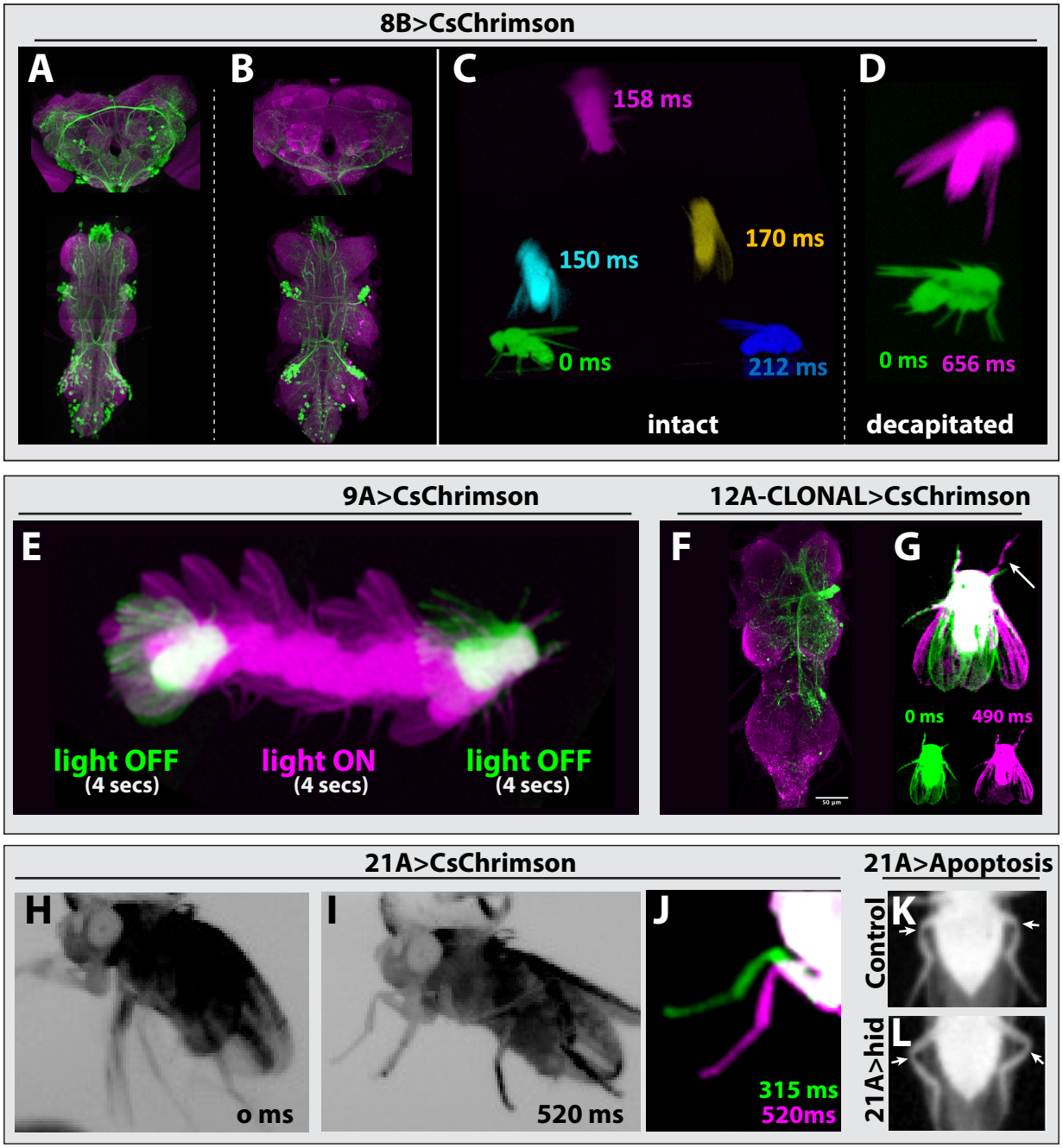
8B>CsChrimson
A
B
C
158 ms
170 ms
150 ms
0 ms
212 ms
intact
D
0 ms
656 ms
decapitated
9A>CsChrimson
E
light OFF
(4 secs)
light ON
(4 secs)
light OFF
(4 secs)
12A-CLONAL>CsChrimson
F
G
0 ms
490 ms
21A>CsChrimson
H
o ms
I
520 ms
J
315 ms
520ms
21A>Apoptosis
Control
K
21A>hid
L

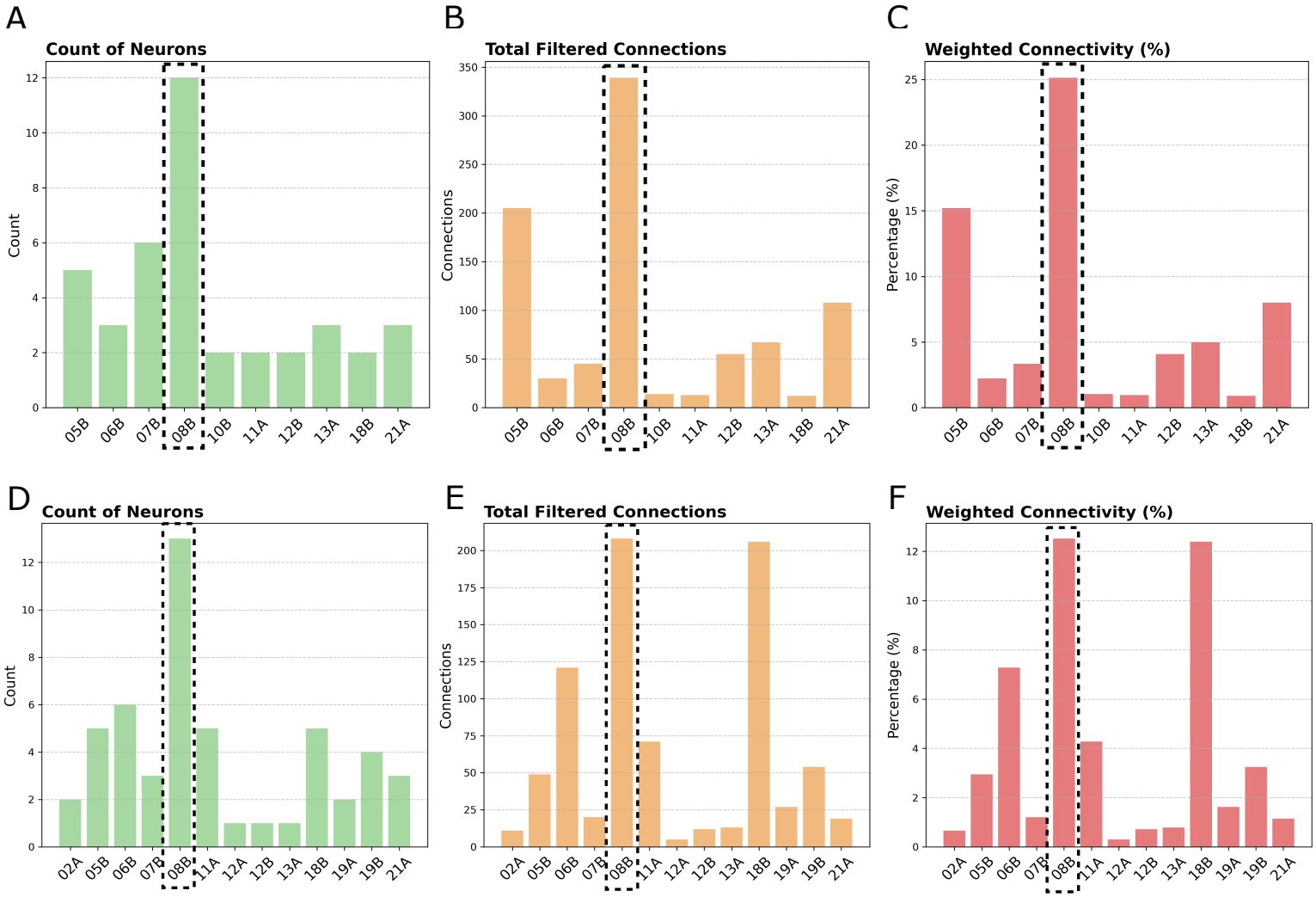
A
Count of Neurons
Count
05B
06B
07B
08B
10B
11A
12B
13A
18B
21A
B
Total Filtered Connections
Connections
C
Weighted Connectivity (%)
Percentage (%)
D
Count of Neurons
Count
02A
05B
06B
07B
08B
11A
12A
12B
13A
18B
19A
19B
21A
E
Total Filtered Connections
Connections
F
Weighted Connectivity (%)
Percentage (%)

Table 1_ GF input

Hemilineage	Neuron Count	Connections	Weighted Connectivity (%)
05B	5	205	15.20
06B	3	30	2.22
07B	6	45	3.34
08B	12	339	25.13
10B	2	14	1.04
11A	2	13	0.96
12B	2	55	4.08
13A	3	67	4.97
18B	2	12	0.89
21A	3	108	8.01

Types
AN05B006, AN05B006, IN05B032, IN05B032, AN05B006
IN06B016, N06B056, IN06B059
IN07B066, IN07B054, IN07B055, IN07B066, IN07B055, IN07B007
AN08B098, AN08B098, AN08B098, AN08B098, AN08B098, AN08B098, AN08B098, AN08B098, AN08B102, AN08B099, AN08B099, IN08B075
AN10B019, AN10B019
IN11A001, IN11A001
IN12B015, IN12B015
IN13A032, IN13A022, IN13A022
IN18B034, IN18B034
IN21A032, IN21A027, IN21A034

Table 2_GF output

hemilineage	Neuron Count	Connections	Weighted Connectivity (%)	Types
02A	2	11	0.66	AN02A002, AN02A002
05B	5	49	2.95	AN05B006, AN05B006, IN05B032, IN05B032, IN05B089]
06B	6	121	7.28	IN06B008, IN06B008, IN06B008, IN06B029, IN06B056, IN06B008
07B	3	20	1.20	IN07B080, IN07B080, IN07B080
08B	13	208	12.52	IN08B003, AN08B09, AN08B098, AN08B098, AN08B098, AN08B098, AN08B098, AN08B098, AN08B009, AN08B099, AN08B099, AN08B009, AN08B098
11A	5	71	4.27	IN11A001, IN11A021, IN11A001, IN11A044, IN11A032
12A	1	5	0.30	IN12A030
12B	1	12	0.72	IN12B015
13A	1	13	0.78	IN13A032
18B	5	206	12.39	IN18B034, IN18B034, IN18B034, AN18B053, IN18B031
19A	2	27	1.62	IN19A117, IN19A106
19B	4	54	3.25	AN19B019, AN19B019, IN19B067, AN19B001
21A	3	19	1.14	IN21A032, IN21A027, IN21A034

Lineage	Clusters (Allen et al.)	Markers	Driver line Combinations
0A	22, 88, 112	En, Inv, Fkh, Tj, Lim1, grn,HLH3B, Mab-21, Gad1	inv-GAL4-DBD, tj-p65.AD: * * * * fkh-GAL4-DBD, tj-p65.AD: * * * * mab21-p65.AD, fkhGAL4-DBD: * * *
1A	16	Dr, Ets21C, Ptx1, ChAT	Dr-p65.AD, ets21C-GAL4-DBD: * * *
1B	12, 47	HLH4C, H15, Mid, Gad1	HLH4C-GAL4-DBD, H15-p65.AD: * * *
2A	15, 86	HLH3B, Oc, Sox21a, Drgx, Lim1, grn, svp, VGlut	sox21a-GAL4-DBD, VGlut-p65.AD: * * * * sox21a-GAL4-DBD, lim1-VP16.AD: * * *
3A	7, 37, 85	H15, HGTX, Grn, Lim1, ChAT	H15-p65.AD, ChaT-GAL4-DBD: *
3B	26	Fer3, CG4328, Gad1	fer3-GAL4-DBD, cg4328-p65.AD: *
4B	0, 100	Exex, Ap, Fkh, Tey, HGTX, HLH4C, Oc, ChAT	ap-p65.AD,fkhGAL4-DBD: * * * ap-p65.AD,hgtx-GAL4-DBD: * * * *
5B	20, 87, 97	Vg, Toy, Vsx2, Lim1, Gad1	vg-p65.AD,toy-GAL4-DBD: * * * *
6A	9, 28	Mab-21, Toy, Gad1	mab21-p65.AD,toy-GAL4-DBD: * *
6B	3, 89	Vg, Sens-2, En, CG4328, Vsx2, Gad1	sens2-p65.AD, vg-GAL4-DBD sens2-GAL4-DBD, vg-p65.AD: * * CG4328-p65.AD, vg-GAL4-DBD: * * *
7B	2, 62	Unc-4, Sv, Mab-21, ChAT	unc-4-p65.AD, mab21-GAL4-DBD: * * * unc-4-GAL4-DBD, sv-p65.AD: * * *
8A	6, 69, 110	Ey, Ems, Toy, Ets65A, VGluT	ems-GAL4-DBD, eyAD: * * * * ems-GAL4-DBD, toy-p65.AD: * * ems-GAL4-DBD, vGluT-p65.AD: * * *
8B	8, 53, **76** (contains cells from 9B)	C15, Lim3, Acj6, ChAT	C15-p65.AD, lim3-GAL4-DBD: * * *
9A	31, 50, 56, 57	Dr, Ets65A, grn, sox21a, Gad1	Dr-p65.AD, gad1-GAL4-DBD: * * * * Dr-p65.AD, sox21a-GAL4-DBD: * * * *
9B	54, **76** (contains cells from 8B)	Lim3, Drgx, Sens-2, Acj6, Tup, HLH4C,VGluT	acj6-p65.AD,VGluT-GAL4-DBD: * * *
10B	39, 68, 91	Exex, Kn, Sens-2, Lim3,ChAT	knot-p65.AD, hb9-GAL4-DBD: * * * * hb9-p65.AD, sens-2-GAL4-DBD: * * * * knot-p65.AD, nkx6-GAL4-DBD: * * * * knot-p65.AD, lim3-GAL4-DBD: * * *
11A	21	Unc-4, Tey, ChAT	unc-4-GAL4-DBD, tey-VP16: * * * unc-4-p65.AD, hgtx-GAL4-DBD: * * *
11B	38	Eve, HLH4C, Gad1	eve-p65.AD, gad1-GAL4-DBD: * * * *
12A	40	Unc-4, TfAP-2, Grn, ChAT	unc-4-GAL4-DBD, TfAP2-p65.AD: * * *
12B	30, 73, 81, 83, 94	Fer3, HGTX, CG4328, H15, Tey, Gad1	HGTX-GAL4-DBD, gad1-p65.AD: * *
13A	48, 75, 79	Dbx, Fer2, Dmrt99B, Gad1	dbx-GAL4-DBD, dmrt99B-p65.AD: * *
13B	17 , 25	D, Vg, CG4328, tey, svp, Gad1	vg-GAL4-DBD, D-VP16.AD: * * vg-GAL4-DBD, tey-VP16.AD: * * *
14A	13, 41, 74	Dr, Toy, Lim1, Ets65A, Grn, VGluT,	Dr-p65.AD, toy-GAL4-DBD: * * *
15B	36, 52, 80	Tup, Lim3, HGTX, VGlut	HGTX-GAL4-DBD, VGlut-p65.AD: * * * nkx6- GAL4-DBD, twit-p65.AD: * * *
16B	5, 46	Lim3, Exex, Bi, Sp1, VGlut,	hb9-p65.AD, bi-GAL4-DBD: * * * hb9-p65.AD, VGlut-GAL4-DBD: * * *
17A	58, 77	Unc-4, Hmx, Tup, ChAT	unc-p65.AD, hmx-GAL4-DBD: * * * *

18B	N/A	Unc-4, ChAT	**No line**
19A	19, 59, 82	Dbx, Fer2, Scro, Gad1	dbx-GAL4-DBD, scro-p65.AD: * * *
19B	27, 71	Unc-4, Otp, ChAT	**No line**
20/22A	14, 33, 34, 78, 108	Bi, Ets65A, Sv, ChAT	sv-p65.AD, ets65-GAL4-DBD: * * * bi-GAL4-DBD, shaven-p65.AD: * * bi-p65.AD, ets65A-GAL4-DBD: * *
21A	1	Dr, Ey, Tj, VGluT	Dr-p65.AD, tj-GAL4-DBD: * * * * Dr-p65.AD, ey-GAL4-DBD: * * *
23B	35, 51, 67, 93	Unc-4, Acj6, Slou, Otp, ChAT	unc-4-p65.AD, acj6-GAL4-DBD: * * *
24B	A small subset of clusters 52 and 36	Toy, Ems, Twit, Vglut	ems-GAL4-DBD, twit-p65.AD: * * *

****: very specific for one hemilineage; *** specific, some contamination from other neurons: ** somewhat specific, significant contribution of e.g .motorneurons or sensory neurons; * More than one hemilineage marked

Hemilineage	Genotype	Phenotype
0A	tj-p65.AD, inv-GAL4-DBD	No apparent behavioral response observed in response to acute optogenetic activation.
1A	Msh-p65.AD, Ets21C-GAL4-DBD	Activation in decapitated animals drove extension of hing leg segments and grooming like, pushing the fly forward, but not causing a clear locomotion. The front and mid legs move as in grooming. Our observation differed from previously observed phenotypes of erratic forward locomotion, occasionally interrupted by grooming in decapitated animals (Harris 2015).
1B	H15-p65.AD, HLH4c-GAL4-DBD	Activation in decapitated flies drives leg rotational movement causing the joint between the femur and tibia to bend laterally, most pronounced by the hind legs. This movement then triggers grooming behavior of the hind legs. Similar phenotype observed in intact flies.
2A	VGlut-p65.AD, Sox21a-GAL4-DBD	Activation in intact animals drove high-frequency wing flapping, consistent with the other research showed the same phenotype with the decapitated flies (Harris, 2015). However, in our experiments with decapitated animals including tethered flies, no wing buzzing was observed, and only halteres moved ventrally upon stimulation and returned to a dorsal position when no longer stimulated. One explanation for this discrepancy is that our driver line appears to target less 2A neurons in the T1 segments.
3A	No specific line	
3B	No specific line	
4B	ap-p65.AD, HGTX-GAL4-DBD	Activation cause the extension of all the legs in both decapitated and intact flies.
5B	vg-p65.AD, toy-GAL4-DBD	Activation of 5B neurons halts almost every movement in the animal, causing walking, grooming, flying (tethered flight assay), and feeding flies to halt these behaviors. After activation, immobile animals reposition their legs to sink lower to the standing surface, consistent with other research (Harris, 2015). Decapitated animals also halt their grooming activity in response to 5B activation. Active 5B neurons also halt the larval locomotion.
6A	No specific line	
6B	CG4328-p65.AD, vg-GAL4-DBD	Activation in intact animals drove inhibition in wing buzzing and leg movements of the tethered flies. Activation in decapitated animals halted sporadic leg movements and drove a subtle change in the posture.
7B	sv-p65.AD, unc-4-GAL4-DBD	Upon 7B activation, both decapitated and intact animals raised their wings and attempted to takeoffs, but they failed. We also observed tibia levetation in response to activation. Harris et al. observed robust take off behavior.
8A	ey-p65.AD, ems-GAL4-DBD	Activation brings the body of the fly closer to the ground likely flexing leg segments in both intact and decapitated animals. Harris et al., 2015 observed minimal effects after activation.
8B	C15-p65.AD, Lim3-GAL4-BD	Activation drove intact animals lean backward and take-off. A few animals initated wing flapping after the jump; others failed to initiate wing flapping and fall after the jump, then they jumped again under the continuous activation. Decapitated animals showed a similar response but never initiated the wing flapping after the take off.
9A	Dr-p65.AD, Gad1-GAL4-DBD	Activation in intact animals drove erratic forward locomotion of the animal. Activation in tethered intact flies resricted the legs to stay in a specific posture.In decapitated animals, bodies were lowered toward the ground with legs becoming more splayed for approximately two seconds before occasional forward locomotion and leg grooming, consistent with previous research (Harris, 2015).
9B	acj6-p65.AD, VGlut-GAL4-DBD	Activation in intact animals drove a subtle phenotype of leg irritation causing bouts of leg grooming of both front and back legs or erratic gait when walking. Decapitated animals halted their grooming in response to 9B activation. This halting behavior was less penetrant compared to the halting behavior observed with 5B activation.

10B	Hb9-p65-AD, sens-2-GAL4-DBD	Activation in intact animals drove erratic walking behavior. 10B activation in decapitated animals drove leg extension and body twisting. Our findings differed from Hartis et al., which showed erratic leg movements causing backwards locomotion with occasional wing flicking and buzzing.
11A	tey-VP16.AD, unc-4-GAL-4DBD	Low intensity light activation drove lateral wing waving with occasional jumping, while high intensity activation drove wing buzzing and jumping in intact and decapitated animals.
11B	eve-p65.AD, Gad1-GAL4-DBD	Harris et al., 2015 observed take-off behavior after activation of the 11B neurons. However, upon light activation, we observed wing movements without any take-off behavior. The wings moved from side to side in a buzzing behavior.
12A	TfAP2-p65.AD, unc-4-GAL4-DBD	CsChrimson expression showed a lethal phenotype with no surviving adults. We generated linage clones using TfAP-2-GAL4 . Animals expressing CsChrimson in 12A neurons in one side of the T1 segment showed a single swing movement of the leg that is located on the same side of the animal lineage clone located. We also observed bilateral wing buzzing.
12B	No specific line	
13A	dmrt99B-p.65AD, dbx-GAL4-DBD	Upon light stimulation, intact flies show leg extension. Decapitated flies show a freezing behavior with the legs unable to change positions until after the light stimulation ends.
13B	D-VP16.AD, vg-GAL4-DBD	Intact flies lost control of their legs and fell on their back with uncoordinated leg movements upon activation of 13B neurons. Decapitated flies responded with a postural change and a weak leg extension phenotype.
14A	Dr-p65.AD, toy-GAL4-DBD	Activation caused intact animals to fall on their back with uncoordinated leg movements; flies remaied uncoordinated until the cessation of the stimulus. In decapitated animals, activation drove femur-tibia joint to move anteriorly, most pronounced in the middle legs. We also observed flexion of the legs.
15B	VGlut-p65.AD, HGTX-GAL4-DBD	Upon light stimulation in both intact and decapitated flies, the legs showed a severe flexing phenotype. The legs flexed tightly against the body with the flies falling into a fetal position until after light stimulation ended.
16B	Hb9-p65.AD, Bi-GAL4-DBD	Activation in both intact and decapitated animals drove flexion at the femur tibia joint causing the animal to sink lower to the ground.
17A	unc-4-p65.AD, Hmx-GAL4-DBD	Activation of 17A neurons drove flexion of all the leg segments in both decapitated and intact animals.
18B	No specific line	
19A	scro-p65.AD, dbx-GAL4-DBD	Activation in decapitated animals drove flexion at the tibia-tarsus joint as well as anterior movement of the femur-tibia axis. In contrast, in decapitated flies, we observed extension of the back legs upon activation. In intact animals, we observed severe flexing of the legs against the body. Harris et al., observed a leg-waving phenotype of the T2 legs in decapitated animals after stimulation.
19B	No specific line	
20/22A	No specific line	
21A	Dr-p65.AD, tj-GAL4-DBD	Activation of 21A neurons in decapitated animals drove flexion of the legs bringing the body of the fly closer to the ground. We observed a similar phenotype in intact animals tehered to a pin. Harris et al., observed an uncoordinated movement phenotype upon activation.
23B	unc-4-p65.AD, acj6-GAL4-DBD	Activation caused intact animals to fall on their back due to uncoordinated leg movements and sustained flexion or extension of the leg segments; flies remaied uncoordinated until the cessation of the stimulus.Flies also showed increased groomng activity. Decapitatd animals showed similar responses.
24B	ems-GAL4-DBD, twit-p65.AD	not tested.